

A Consensus Model of Glucose-Stimulated Insulin Secretion in the Pancreatic β -Cell

Deepa Maheshvare M.¹, Soumyendu Raha¹, Matthias König^{2,3,*}, and Debnath Pal^{1,3,*}

¹Department of Computational and Data Sciences, Indian Institute of Science, Bangalore 560012, India

²Institute for Biology, Institute for Theoretical Biology, Humboldt-University Berlin, Philippstraße 13, Berlin, 10115, Germany

³equal contribution

Correspondence*: dpal@iisc.ac.in, konigmatt@googlemail.com

ABSTRACT

The pancreas plays a critical role in maintaining glucose homeostasis through the secretion of hormones from the islets of Langerhans. Glucose-stimulated insulin secretion (GSIS) by the pancreatic β -cell is the main mechanism for reducing elevated plasma glucose. Here we present a systematic modeling workflow for the development of kinetic pathway models using the Systems Biology Markup Language (SBML). Steps include retrieval of information from databases, curation of experimental and clinical data for model calibration and validation, integration of heterogeneous data including absolute and relative measurements, unit normalization, data normalization, and model annotation. An important factor was the reproducibility and exchangeability of the model, which allowed the use of various existing tools. The workflow was applied to construct the first consensus model of GSIS in the pancreatic β -cell based on experimental and clinical data from 39 studies spanning 50 years of pancreatic, islet, and β -cell research in humans, rats, mice, and cell lines. The model consists of detailed glycolysis and equations for insulin secretion coupled to cellular energy state (ATP/ADP ratio). Key findings of our work are that in GSIS there is a glucose-dependent increase in almost all intermediates of glycolysis. This increase in glycolytic metabolites is accompanied by an increase in energy metabolites, especially ATP and NADH. One of the few decreasing metabolites is ADP, which, in combination with the increase in ATP, results in a large increase in ATP/ADP ratios in the β -cell with increasing glucose. Insulin secretion is dependent on ATP/ADP, resulting in glucose-stimulated insulin secretion. The observed glucose-dependent increase in glycolytic intermediates and the resulting change in ATP/ADP ratios and insulin secretion is a robust phenomenon observed across data sets, experimental systems and species. Model predictions of the glucose-dependent response of glycolytic intermediates and insulin secretion are in good agreement with experimental measurements. Our model predicts that factors affecting ATP consumption, ATP formation, hexokinase, phosphofructokinase, and ATP/ADP-dependent insulin secretion have a major effect on GSIS. In conclusion, we have developed and applied a systematic modeling workflow for pathway models that allowed us to gain insight into key mechanisms in GSIS in the pancreatic β -cell.

Keywords: glucose-stimulated insulin secretion, GSIS, glycolysis, pancreas, kinetic model, systems biology

1 INTRODUCTION

- 1 The pancreas plays a vital role in maintaining
- 2 glucose homeostasis (Woods et al., 2006) through
- 3 the secretion of hormones from the islets of

Langerhans. The most important hormones are insulin, secreted by the pancreatic β -cells, and glucagon, secreted by the α -cells, both of which play

4
5
6

7 key roles in regulating glucose homeostasis (König
8 et al., 2012a).

9 Glucose-induced insulin secretion (GSIS) is
10 a physiological process by which the pancreas
11 releases insulin in response to an increase in blood
12 glucose levels. When glucose enters the bloodstream
13 after a meal, it is taken up by β -cells in the
14 pancreas through glucose transporters, primarily
15 GLUT2 (MacDonald et al., 2005). Once inside the
16 β -cells, glucose is metabolized via glycolysis, which
17 produces energy in the form of ATP.

18 The coupling of glycolysis with the insulin
19 secretion mechanism in the β -cell is established by
20 the regulatory effects of glycolytic intermediates
21 on the levels of energy metabolites such as ATP
22 and NADH (Newsholme et al., 2014; Prentki
23 et al., 2013). The rise in ATP levels triggers
24 a series of events that lead to the release of
25 insulin. Specifically, the high ATP levels close
26 ATP-sensitive potassium channels (Ashcroft, 2006),
27 which leads to depolarization of the cell membrane
28 and opening of voltage-gated calcium channels. The
29 influx of calcium triggers the exocytosis of insulin-
30 containing vesicles, leading to the release of insulin
31 into the bloodstream (Rorsman and Braun, 2013;
32 Guerrero-Hernandez and Verkhratsky, 2014). The
33 K_{ATP}/Ca^{2+} independent signaling mechanisms
34 and the other metabolites besides glucose contribute
35 to the amplification of the signaling events that
36 trigger insulin secretion (Guay et al., 2013).

37 GSIS by the pancreatic β -cell is the primary
38 mechanism for lowering elevated plasma glucose
39 levels. The amount of insulin released increases
40 with the glucose in the bloodstream. This process
41 is crucial for the regulation of blood glucose levels
42 by promoting the uptake and use of glucose by cells
43 throughout the body, such as muscle, fat tissue, and
44 the liver (Di Camillo et al., 2014; Fritzsche et al.,
45 2008).

46 Glycolysis is the primary metabolic pathway
47 responsible for GSIS. It involves the uptake of
48 glucose and its conversion to pyruvate, which is
49 critical for ATP synthesis and maintenance of ATP
50 levels. Experimental data from metabolic profiling

51 studies in islet cells support the key role of glycolysis
52 in GSIS (Spégel et al., 2013, 2015; Taniguchi et al.,
53 2000). As glucose levels increase, glycolytic flux
54 and most glycolytic intermediates increase in a dose-
55 dependent manner. Changes in adenine nucleotide
56 levels due to variations in glycolytic flux lead
57 to changes in nucleotide ratios, with increasing
58 glucose levels resulting in a positive correlation
59 between the ATP/ADP ratio and Ca^{2+} response
60 and insulin release. This trend is consistent across
61 several studies (Detimary et al., 1996; Malaisse
62 et al., 1978; Salvucci et al., 2013), including isolated
63 islets perfused with glucose, rat and mouse tissue
64 homogenates, and insulin-secreting cell lines. The
65 increase in ATP/ADP ratio ranges from 2 to 7
66 when glucose levels are increased from 2.8mM
67 to 30mM, indicating similar behavior in different
68 experimental systems studying insulin secretion by
69 the pancreas (Huang and Joseph, 2014).

70 Mathematical models have been developed
71 to investigate the metabolic and signaling
72 mechanisms that trigger and amplify insulin
73 secretion. Early models of β -cells focused on
74 examining the relationship between glycolytic
75 oscillations and pulsatile insulin release to
76 understand GSIS (Bertram et al., 2007; Tornheim,
77 1997). Merrins et al. analyzed the oscillations in
78 glycolytic intermediates (i.e. fructose-6-phosphate,
79 fructose-2,6-bisphosphate, and fructose-1,6-
80 bisphosphate) and their effect on pulsatile insulin
81 secretion (Merrins et al., 2012), while other models
82 integrated glycolytic flux with mitochondrial ATP
83 production to study the role of reducing equivalents
84 such as pyridine nucleotides in enhancing insulin
85 secretion (Westermark et al., 2007; Bertram et al.,
86 2006). Jiang et al. further combined previously
87 developed models of glycolysis, citric acid cycle, β -
88 oxidation, pentose phosphate shunt, and respiratory
89 chain and studied the local and global dynamics
90 of the GSIS mechanism in response to parameter
91 perturbations. These models were coupled with the
92 calcium signaling pathway of Fridlyand et al. to
93 create an integrated metabolic model (Fridlyand
94 and Philipson, 2010; McKenna et al., 2016).

To investigate the synergistic insulinotropic effect of other nutrient sources, Salvucci et al. (Salvucci et al., 2013) developed a model by integrating alanine metabolism with glucose metabolism, the citric acid cycle, and the respiratory chain. Gelbach et al. developed a system of 65 reactions integrating glycolysis, glutaminolysis, the pentose phosphate pathway, the citric acid cycle, the polyol pathway, and the electron transport chain to study the kinetics of insulin secretion (Gelbach et al., 2022).

However, the majority of these models are based on earlier models that were developed using kinetic data from organisms other than humans or non-pancreatic tissues, such as a glycolysis model that utilized kinetic data from experiments on yeast cell extract, or a glycolysis model based on kinetic data from mammalian muscle (Smolen, 1995). Often, the data used to build these models is limited and comes from a single experimental study. In most models specific to β -cells, reaction kinetics are described by simple mass-action rate laws. There exists no detailed kinetic model of the changes in glycolysis during GSIS that can effectively integrate the observed changes in glycolytic and energy intermediates from a wide range of GSIS experiments.

In systems biology and systems medicine, ensuring the reproducibility of computational models and integrating diverse data from multiple sources into these models are critical challenges. Standards for model description, such as the Systems Biology Markup Language (SBML) (Hucka et al., 2015; Keating et al., 2020), have been developed to enable the reusability and reproducibility of existing models, but they have yet to be utilized in the field of pancreatic GSIS modeling. Furthermore, there is a need to address how to integrate heterogeneous data from different studies conducted in different organisms and experimental systems in the context of GSIS modeling.

This study aims to develop a detailed kinetic model of GSIS and the associated changes in glycolysis in the pancreatic β -cell. The novel contributions of this

work include a systematic curation and integration of changes in glycolytic metabolites from different experimental studies across different species and experimental systems. Based on this unique data set, a detailed kinetic model of glycolysis and GSIS was constructed using a systematic approach with a focus on reproducibility. This approach allowed the establishment of a consensus model of the changes that occur in insulin secretion with varying glucose concentrations. The overall goal was to provide a better understanding of the mechanisms underlying GSIS and to contribute to the development of improved computational models of these processes.

2 RESULTS

Our study introduces a detailed kinetic model of GSIS in the pancreatic β -cell, which has the ability to simulate alterations in glycolytic intermediates and ATP/ADP ratio due to glucose levels and the effect of change in the energy state of the β -cell on insulin secretion.

2.1 Systematic curation of data set of changes in GSIS

In the course of this study, we compiled a comprehensive data set (Tab. 1) of GSIS based on experimental and clinical data from 39 studies spanning half a century of research on pancreatic, islet, and β -cell function in humans, rats, mice, and cell lines. Specifically, we systematically curated metabolomics data from studies conducted between 1970 and 2020, comprising information on the concentration of glycolytic intermediates and cofactors in both time-course and steady-state experiments, as well as the corresponding glucose doses. The data set contains 17 metabolites, comprising 359 data points from steady-state experiments and 249 data points from time-course studies. It includes both absolute and relative measurements of metabolite changes, and an overview of the available information for each metabolite and study is presented in Fig. 1.

This data set represents the first open and FAIR (findable, accessible, interoperable, and

180 reusable) large-scale collection of data on changes in
181 glycolysis and insulin secretion in the pancreatic β -
182 cell during GSIS. We used the absolute and relative
183 measurements of glycolysis metabolites and insulin
184 secretion rates in this data set for model calibration
185 and evaluation.

186 The data set is available under a CC-BY4.0 license
187 from <https://github.com/matthiaskoenig/pancreas->
188 model.

189 2.2 Reproducible modeling workflow

190 In this study, we describe a comprehensive
191 modeling workflow for building small kinetic
192 pathway models (Fig. 2) using SBML (Hucka et al.,
193 2015; Keating et al., 2020).

194 In our model-building workflow, we followed
195 several steps to construct a kinetic SBML model
196 of glycolysis. A) First, we built an SBML model
197 based on glycolytic reactions and intermediates from
198 existing models and pathway databases. B) We then
199 annotated metabolites and reactions with metadata
200 information which was extended by querying VMH
201 and the BiGG database, resulting in mappings
202 to additional resources such as HMDB, BioCyc,
203 MetaNetX, ChEBI, and SEED. C) We collected
204 and retrieved kinetic parameters such as K_M , K_I ,
205 K_A , and K_{eq} constants from databases and D)
206 integrated them with synonyms associated with
207 each queried metabolite using compound identifier
208 mapping services. E) We integrated the resulting
209 parameters and assigned median values to the
210 model parameters. F) Next, we curated data from
211 studies reporting metabolite concentrations and
212 changes, and insulin secretion in pancreatic, islet,
213 and β -cell lines through a literature search. G)
214 Unit normalization was then performed to convert
215 reported metabolite concentrations and insulin
216 secretion to mmole/l (mM) and nmole/min/ml (β -
217 cell volume), respectively. H) Data normalization
218 was performed to remove systematic differences
219 between data reported in different studies and
220 experimental systems. I) Next, values for kinetic
221 parameters, initial concentrations, volumes, rate
222 equations, and annotations were integrated into

the stoichiometric model. J) We calibrated the
223 model by parameter optimization using time-course
224 and steady-state data and K) generated the final
225 SBML kinetic model using all the information.
226 L) Finally, we performed model predictions of
227 glycolytic intermediates and insulin response as a
228 function of varying glucose concentrations. Steps
229 were performed iteratively to fill gaps and extend
230 the data set and model.
231

232 2.3 Computational model

Using the established data set, we utilized
233 the aforementioned workflow to develop the first
234 consensus model of GSIS in the pancreatic β -cell.
235 The model is comprised of detailed glycolysis and
236 equations for insulin secretion which are coupled
237 to the cellular energy state (ATP/ADP ratio). The
238 metabolites and reactions incorporated into the
239 kinetic model are depicted in Fig. 3, and their
240 biochemical interactions are represented through
241 a system of ordinary differential equations. The
242 model consists of 21 enzyme-catalyzed reactions,
243 25 metabolites, and 91 parameters, and also includes
244 an empirical model that connects the energy state
245 of the β -cell to insulin secretion.
246

When glucose levels are high, GLUT transporter
247 allows glucose to enter the cell, and glucokinase
248 converts glucose to glucose-6-phosphate. The
249 upper glycolysis produces fructose-6-phosphate,
250 fructose-1,6-phosphate, and triose phosphates like
251 dihydroxyacetone phosphate and glyceraldehyde
252 phosphate. Lower glycolysis then leads to the
253 creation of 3-phosphoglycerate, 2-phosphoglycerate,
254 phosphoenolpyruvate, and pyruvate. Pyruvate can
255 be transformed into lactate or transported to the
256 mitochondria. For each glucose molecule, two ATP
257 molecules are produced. Changes in ATP/ADP ratio
258 trigger insulin secretion.
259

The SBML model is available
260 under a CC-BY4.0 license
261 from <https://github.com/matthiaskoenig/pancreas->
262 model.
263

264 2.4 Normalization of data

265 The aim of this study was to investigate
266 variations in glycolysis, glycolytic intermediates,
267 energy metabolites, and insulin secretion during
268 GSIS using the established model. In order to
269 integrate heterogeneous experimental data for each
270 metabolite and insulin secretion rate, we conducted
271 a two-step normalization process to standardize
272 time course and dose-response measurements. The
273 normalization process involved unit normalization
274 (as discussed in Sec. 4.7) and data normalization (as
275 discussed in Sec. 4.8) to normalize the diverse data
276 and eliminate systematic deviations for individual
277 studies. We present the case of glucose 6-phosphate
278 as an example of the normalization process (see
279 Fig. 4). The experimental curves were converted
280 to relative (fold) and unit-normalized absolute
281 measurements (Fig. 4A and Fig. 4B). To combine
282 the fold data and absolute data, we multiplied
283 the fold values by the basal concentration to
284 obtain absolute values (Fig. 4C). If the basal
285 metabolite concentration was not reported, we
286 used the mean curve of the absolute data at the
287 pre-incubation glucose dose of the experiment
288 to determine the basal value. For metabolites
289 consisting of only relative measurements, we used
290 the half-saturation K_m value of the metabolite as
291 an estimate for the basal concentration. Using
292 this strategy, we converted all fold-changes and
293 time courses to absolute data with standardized
294 units, which was then combined with the existing
295 absolute data. However, the standard deviation of
296 the combined data set measurements was high, and
297 large systematic differences between studies could
298 be observed. We determined scaling factors for
299 every study to minimize the difference between
300 all studies based on least-squares minimization (as
301 discussed in Sec. 4.8.1). The resulting normalized
302 data (Fig. 4D) was then used for model calibration.
303 We applied this procedure to all metabolites in the
304 model as well as the insulin secretion rate, reducing
305 the variability in the data substantially.

2.5 Changes in glycolytic metabolites and insulin secretion in GSIS

307

Our work has uncovered several key findings related to GSIS. First, we found that almost all glycolytic intermediates increase in a glucose-dependent manner across a wide range of glucose concentrations, as illustrated in Figures 5, 6, and 7. This increase in glycolytic intermediates is accompanied by a corresponding increase in energy metabolites, especially ATP and NADH. However, one notable exception is ADP, which decreases with increasing glucose levels. As a result, there is a significant increase in ATP/ADP ratios in β -cells with increasing glucose, a key factor in insulin secretion. This phenomenon is robust across different data sets, experimental systems, and species. An important observation is that not only ATP and NADH increase with increasing glucose, but also the total ATP (ATP + ADP) and total NADH (NAD + NADH).

Our model was able to predict the glucose-dependent response of glycolytic intermediates and insulin secretion with good agreement to most experimental measurements, as summarized in Table 1. We observed a dose-dependent increase in glycolytic intermediates when glucose concentrations were increased from 0.01 mM to 35 mM. The model predicts that steady states of glycolytic metabolites under constant glucose are reached after approximately 20 minutes, with only 5-10 minutes required to reach steady state according to our simulations.

Figure 8A illustrates the relationship between glucose dose and insulin release, while Figure 8B shows the effect of varying the ATP/ADP ratio on the insulin response. Specifically, the ATP and ADP concentrations of the β -cell increase and decrease, respectively, with the external glucose dose, resulting in an increased ATP/ADP ratio that triggers insulin release. The model is able to reproduce the steady-state insulin secretion depending on glucose concentration, but fails to describe the fast initial insulin release.

349 2.6 Sensitivity analysis of parameters 350 affecting GSIS

351 To determine how the model parameters affect
352 the rate of insulin release, we performed a local
353 sensitivity analysis (Sauro, 2020). Figure 8C shows
354 the sensitivity of insulin flux to a 10% change
355 in model parameter values at different glucose
356 concentrations. The rate of insulin secretion depends
357 on the ATP/ADP ratio, so perturbing parameters
358 that affect ATP formation and consumption has
359 strong effects. Figure 8D shows the highly sensitive
360 parameters that have positive and negative effects
361 on insulin secretion, including factors affecting
362 ATP consumption, ATP formation, hexokinase,
363 phosphofructokinase, and ATP/ADP-dependent
364 insulin secretion.

365 In conclusion, our systematic pathway modeling
366 workflow provides insights into the key mechanisms
367 of GSIS in the pancreatic β -cell.

3 DISCUSSION

368 We have developed a comprehensive kinetic
369 model of GSIS in the pancreatic β -cell that can
370 simulate glucose-dependent changes in glycolytic
371 intermediates, ATP/ADP ratio, and their effect
372 on insulin secretion. The main objective of this
373 study was to establish a standardized workflow for
374 data integration and normalization to construct a
375 tissue-specific model of glycolysis and GSIS in the
376 β -cell. Although we did not model other important
377 pathways related to ATP homeostasis, such as the
378 citric acid cycle, the pentose phosphate pathway,
379 and the respiratory chain, our workflow can be
380 easily extended to include them. Incorporating
381 these pathways into our model will enable us to
382 explicitly model the regulatory effect of downstream
383 metabolites on the ATP/ADP ratio and insulin
384 secretion. Previous studies have shown that fatty
385 acids and amino acids can also induce insulin
386 secretion in addition to glucose. Therefore, linking
387 glucose metabolism with fatty acid and amino
388 acid metabolism could help in understanding the
389 insulinotropic effects of other fuel sources.

The increase in ATP levels triggers a cascade 390 of events that culminate in the release of 391 insulin from β - cells. Precisely, high ATP levels 392 prompt the closure of ATP-sensitive potassium 393 channels (Ashcroft, 2006). Consequently, the 394 cell membrane depolarizes, opening voltage-gated 395 calcium channels, which allows calcium influx. The 396 influx of calcium triggers exocytosis of insulin- 397 containing vesicles, leading to the release of insulin 398 into the bloodstream (Rorsman and Braun, 2013; 399 Guerrero-Hernandez and Verkhratsky, 2014). These 400 electrophysiological changes resulting in insulin 401 secretion were not modeled explicitly, but the 402 effect of the ATP/ADP ratio on insulin secretion 403 was modeled using a phenomenological (Hill-type) 404 expression. Consequently, the model's predictive 405 capacity is limited to the steady-state glucose- 406 insulin secretion dynamics. Expanding the model 407 to explicitly describe these phenomena would 408 allow to study experimentally observed patterns 409 such as biphasic insulin secretion (Pedersen et al., 410 2008). Of note, the dynamics changing glycolytic 411 intermediates were correctly described by the 412 model. 413

Although our model has some limitations, it 414 represents the first data-driven approach to integrate 415 information from diverse sources and experimental 416 setups. Moreover, it provides the first systematic 417 analysis of the glycolytic changes that occur during 418 insulin secretion in response to different glucose 419 levels. Our study reveals that in GSIS, almost 420 all glycolytic intermediates increase in a glucose- 421 dependent manner as do total ATP and NADH, 422 which is a significant finding. 423

Our model was developed to address the 424 limitations of existing pancreatic β -cell models 425 of glucose-insulin kinetics. These models often 426 suffer from several drawbacks such as limited 427 evaluation to a single data set, non-standardized 428 formats of experimental data and kinetic parameters, 429 and non-reproducible formats. To overcome these 430 limitations, we have created open, free, and FAIR 431 assets that can be used for the study of pancreatic 432 physiology and GSIS. These assets include a fully 433 reproducible SBML model of pancreatic β -cell 434

glycolysis, a data curation workflow, strategies for unit and data normalization, and a large database of metabolic data of the pancreatic β -cell. Our systematic model-building workflow can be used as a blueprint to construct reproducible kinetic models of cell metabolism.

Computational modeling faces a significant challenge due to the substantial variation in data across different experimental systems, species, and cell lines. Often, relative data instead of absolute data is reported, further complicating the task of data integration. In this study, we developed a reliable data normalization workflow that was applied to experimental and clinical data from 39 studies conducted over the past 50 years on pancreatic, islet, and β -cell function in various species and cell lines. Our approach substantially reduced data heterogeneity and revealed a highly consistent response in glycolytic metabolites and insulin secretion. The high degree of conservation in the system of GSIS may have contributed to the effectiveness of the normalization workflow, as similar mechanisms are at play in different species, and the general changes can be observed across various experimental systems.

The study has laid a strong groundwork for enhancing our comprehension of the underlying reasons behind impaired insulin secretion. By mapping proteomics or transcriptomics data onto specific pathways, the developed model could be utilized to gain further insight into changes in GSIS, for instance in diabetic patients.

Furthermore, this model can serve as a crucial component for physiological whole-body models of glucose homeostasis, allowing researchers to investigate the relationship between insulin release and glucose uptake by insulin-responsive tissues.

In conclusion, this study utilized a systematic modeling workflow to gain insight into the key mechanisms involved in glucose-stimulated insulin secretion (GSIS) in pancreatic β -cells. When extended for translational purposes in clinical settings, it can serve to create reference models to identify variations in subjects which can lead to

useful inferences regarding underlying metabolic conditions with therapeutic relevance.

4 METHODOLOGY

The workflow for building the kinetic model is illustrated in Fig. 2, with the following sections providing information on the individual steps.

4.1 Stoichiometric model

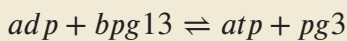
Chemical formulas and charges were assigned to all metabolites, and reactions were examined to ensure that they maintained mass and charge balance. The kinetic model encompasses glycolytic reactions and correlates the energy status of the β -cell with insulin secretion. sbmlutils (König, 2022c) was used to create and validate the model, while cy3sbml (König et al., 2012b) was used to confirm its coherence. The mass and charge balance of the system was verified using cobrapy (Ebrahim et al., 2023).

4.2 Metadata integration

Adding semantic annotations to models is an essential aspect of improving their interoperability and reusability, as well as facilitating data integration for model validation and parameterization (Neal et al., 2019, 2020). To describe the biological and computational significance of models and data in a machine-readable format, semantic annotations are encoded as links to knowledge resource terms. Open modeling and exchange (OMEX) metadata specifications were employed to annotate model compartments, species, and reactions with metadata information (Fig. 2B).

Case study: Phosphoglycerate kinase

The enzyme phosphoglycerate kinase (*PGK*) catalyses the conversion of 1,3-biphosphoglycerate (*bpg13*) and ADP to form 3-phosphoglycerate (*pg3*) and ATP.



In our model, PGK is described by the following annotations:

SBO:0000176, vmhreaction/PGK, bigg.reaction/PGK, kegg.reaction/R01512, ec-code/2.7.2.3, biocyc/META:PHOSGLYPHOS-RXN, uniprot:P00558, uniprot:P07205.

510

The model components, including physical volumes, reactions, metabolites, and kinetic-rate laws, were annotated using Systems Biology Ontology (SBO) terms, which describe the computational or biological meaning of the model and data (Courtot et al., 2011). Biomedical ontology services such as Ontology Lookup Service (OLS) (Cote et al., 2010), VMH (Noronha et al., 2019), and BiGG (King et al., 2016) were used to collect these terms. Additional information for species and reactions were gathered from various databases such as HMDB, BioCyc, MetaNetX, ChEBI, and SEED. For instance, the model's metabolites were annotated with identifiers from VMH, BiGG, KEGG, HMDB, BioCyc, ChEBI, MetaNetX, and SEED, while reactions were annotated with VMH, Rhea, MetaNetX, SEED, BiGG, BioCyc, and KEGG identifiers (Hari and Lobo, 2022). Enzymes catalyzing reactions were annotated with identifiers from enzyme commission (EC) numbers, UniProt (The UniProt Consortium, 2017), and KEGG. Finally, the annotations were incorporated into the SBML file using sbmlutils (König, 2022c) and pymetadata (König, 2022b).

Case study: 1,3-biphosphoglycerate

There is currently a bottleneck in data integration due to the use of multiple synonyms to refer to a single compound in data repositories. For instance, *bpg13* is identified by different names in SABIO-RK (*Glycerate 1,3-bisphosphate, 3-phospho-D-glyceroyl phosphate*) and BRENDA (*3-phospho-D-glyceroyl phosphate*). Additionally, the labeling of *1,3-biphosphoglycerate*, abbreviated as *DPG*, varies across existing β -cell models (e.g., *1,3-bisphospho-D-glycerate* in (Jiang et al., 2007) and *1,3-biphosphoglycerate* in (Salvucci et al., 2013)). Overall, *bpg13* is associated with seven synonyms: *1,3-Bisphospho-D-glycerate*, *13dpg*, *3-Phospho-D-glyceroylphosphate*, *Glycerate 1,3-bisphosphate*, *3-phospho-d-glyceroylphosphate*, *1,3-diphosphoglyceric acid*, *3-Phospho-D-glyceroyl phosphate*. This issue makes it difficult to integrate data and information from different resources, highlighting the need to link chemical entities in the model to knowledge resource terms.

In our model, *bpg13* is clearly described by the following metadata annotations: SBO:0000247, vmhmetabolite/13dpg, bigg.metabolite/13dpg, kegg.compound/C00236, biocyc/META:DPG, CHEBI:16001, inchikey:LJQLQCAXBUHEAZ-UWTATZPHSA-N.

The formula and charge of *bpg13* are C3H4O10P2 and -4, respectively.

536

4.3 Kinetic parameters

537

Kinetic parameters, such as half-saturation constants (K_M), inhibition constants (K_I), activation constants (K_A), and equilibrium constants (K_{eq}), were gathered from literature and a variety of databases (see Fig. 2C). Values were programmatically accessed

from UniProt (The UniProt Consortium, 2017), BRENDA (Placzek et al., 2017) using brendapy (König, 2022a), and SABIO-RK (Wittig et al., 2018). These databases were searched using an organism's NCBI taxonomy identifier and reaction EC number as input search terms. Various parameters, including measurement type (K_m , K_i , and K_a), experimental conditions (pH, temperature), KEGG reaction identifiers, enzyme type (wildtype or mutant), associated metabolite identifiers (SABIO compound name or BRENDA ligand id), UNIPROT identifiers associated with the isoforms of an enzyme, source tissue, and details of data source (PubMed identifier) were obtained. Since there is limited availability of kinetic data for *Homo sapiens*, we also searched for parameter values reported in studies of animal species that are closely related to humans and utilized them if no data were available for humans.

4.4 Synonym mapping

To map compound synonyms associated with each queried metabolite, we utilized compound identifier mapping services and available metadata annotations. First, we associated the name of each compound with internal database identifiers, such as the internal identifier of Glycerone-phosphate in SABIO, which is 28. Then, we linked the internal identifiers to external identifiers, such as those from ChEBI and KEGG. The external identifiers associated with the SABIO ligand identifier were obtained from cross-ontology mappings available in SABIO-RK. Similarly, we queried the REST API of UniChem to obtain the external identifiers associated with the BRENDA ligand identifier. By doing so, we were able to map most of the kinetic parameters to their respective compounds (Fig. 2D).

4.5 Model parameters

For each parameter in the model, the median value was calculated after synonym mapping and the values were assigned to the model parameters, see Fig. 2E. This was performed for initial concentrations, equilibrium K_{eq} constants,

half-saturation constants K_m , inhibition K_i , and activation K_a constants.

4.6 Data curation

The next step involved curating data from studies that reported metabolite values, insulin secretion, or maximal velocities of glycolytic reactions V_{max} in pancreatic, islet, and β -cell lines (Fig. 2F). Relevant studies were identified through a literature search in PubMed, with a focus on time course and dose-response profiles of metabolite concentrations for metabolites and insulin secretion. Tissue homogenates were prepared by isolating islets from rodents, humans, or insulin-secreting cell lines (see Tab. 1). Assays were performed by stimulating the medium with various pre-incubation and incubation concentrations of glucose. To curate the data, established curation workflows from PK-DB (Grzegorzewski et al., 2021b), which were applied in a recent meta-analysis (Grzegorzewski et al., 2021a), were used. The numerical data was digitized by extracting the data points from the figures and tables using WebPlotDigitizer (Rohatgi, 2021). The incubation time and glucose concentration of the stimulation medium were recorded for all measurements, and meta-information such as organism and tissue type were documented.

The data is available under a CC-BY 4.0 license from <https://github.com/matthiaskoenig/pancreas-model>. In this study, version 0.9.5 of the data set is used (Deepa Maheshvare and König, 2023).

4.7 Unit normalization

The data measured in different studies is often reported in different units. Therefore, unit normalization was performed to integrate the data and convert metabolite concentrations and insulin secretion to standardized units of mmole/l (mM) and nmole/min/ml (β -cell volume), respectively (Fig. 2G).

Absolute measurements reported in metabolic profiling studies were found in various units such as per gram DNA, per gram wet weight or dry

628 weight of the islet tissue, per cell, per islet, etc. To use these values for model calibration,
 629 both the absolute and relative measurements were
 630 first converted to concentration units in mM. The
 632 absolute values were converted to model units
 633 by multiplying the raw values with appropriate
 634 unit conversion factors. For instance, the islet
 635 content of glucose 6-phosphate, G6P, (pmol/islet)
 636 was converted to concentration units (mM) using
 637 the distribution volume of water in the islet
 638 (2nl/islet) (Ashcroft et al., 1970) as the conversion
 639 factor. Relative measurements were mainly reported
 640 with reference to a basal concentration. These
 641 relative measurements were converted to absolute
 642 quantity by multiplying the fold values with the
 643 respective metabolite concentration at the basal or
 644 pre-incubation concentration of glucose.

645 4.8 Data normalization and integration

646 Data collected from experiments performed in
 647 different laboratories, under different experimental
 648 conditions, and with different animal species
 649 showed significant variability after unit
 650 normalization. Therefore, data normalization was
 651 performed to eliminate systematic discrepancies
 652 between data reported in different studies (as
 653 shown in Fig. 2H). To achieve this, least squares
 654 optimization was used to minimize the distance
 655 between individual experimental curves and
 656 the weighted average of all curves for a given
 657 metabolite. The data normalization process involved
 658 a two-step procedure in which the steady-state
 659 data were first normalized for each metabolite.
 660 The resulting steady-state normalization was then
 661 used to normalize the time course data for that
 662 metabolite (see Fig. 4 for the example of glucose-6
 663 phosphate).

664 4.8.1 Steady-state data normalization

665 Steady-state (ss) experiments consisted of pre-
 666 incubation with one glucose dose followed
 667 by incubation with another glucose dose.
 668 The steady state data of the experiment α ,
 669 ($c_0^\alpha, c_1^\alpha, \dots, c_n^\alpha$) observed at n incubation glucose
 670 doses ($d_0^\alpha, d_1^\alpha, \dots, d_n^\alpha$) is expressed by the piecewise

linear-interpolation function C^{ss} . Here, α belongs to the set of steady-state experiments $1 \leq \alpha_{ss}^{\alpha}$ with $N^{\alpha_{ss}}$ being the number of steady-state experimental curves of the metabolite s .

Mean curve. The mean steady-state curve \bar{C}^{ss} of each metabolite s is calculated as the weighted average of all experimental curves. The data points of the mean curve were interpolated using a piecewise smooth spline function. For data sets consisting of 2 data points, a linear interpolation was used.

We formulate a least-squares optimization problem to minimize the distance between the individual experimental curves and the mean curve \bar{C}^{ss} . The cost function F of the optimization problem is given by,

$$F(f^\alpha) = \sum_{i=1}^n (f^\alpha \cdot C^{ss}(d_i^\alpha) - \bar{C}^{ss}(d_i^\alpha))^2 \quad (1)$$

In Eq. 1, $C^{ss}(d_i^\alpha)$ and $\bar{C}^{ss}(d_i^\alpha)$ are the function values of the individual and mean interpolation function at the i^{th} value of the glucose dose. N is the number of glucose values in the dose-response curve of the experiment α .

For each experimental curve, the factor f^α was determined so that the residual error in Eq. 1 is minimized. The residual error is minimum at the point where the derivative of the cost function F is zero. Taking the partial derivative of Eq. 1 with respect to the scale transformation parameter gives factor f^α of the experimental curve α (Eq. 2).

$$f^\alpha = \frac{\sum C^{ss}(d_i^\alpha) \bar{C}^{ss}(d_i^\alpha)}{\sum (C^{ss}(d_i^\alpha))^2} \quad (2)$$

The scale factors of all steady state curves ($f^1, \dots, f^{N^{\alpha_{ss}}}$) were determined by minimizing the respective cost functions ($F(f^1), \dots, F(f^{N^{\alpha_{ss}}})$). Multiplying the experimental curve C^α by the scaling factor f^α shifts the experimental curve towards the mean curve. A new mean curve can

705 be calculated with the scaled data. The curves were
706 scaled iteratively until all f^α converged.

707 4.8.2 Time course data normalization

708 Time course (tc) experiments consisted of pre-
709 incubation with one glucose dose followed by
710 incubation with another glucose dose. The time-
711 dependent data of the time course experiment
712 β ($c_0^\beta, c_1^\beta, \dots, c_m^\beta$) observed at m time points
713 ($t_0^\beta, t_1^\beta, \dots, t_m^\beta$) is expressed by the piecewise linear-
714 interpolation function C^β . Here, β belongs to the
715 set of time course experiments $1 \leq \beta \leq N^{\beta_{tc}}$ with
716 $N^{\beta_{tc}}$ being the number of time course experimental
717 curves of the metabolite s . For normalization, each
718 time course was scaled by a factor f^β .

719 For a given incubation glucose dose d^β , the
720 metabolite concentration at the last time point
721 $C^{tc}(t_m)$ corresponds to the steady state value reached
722 for the given d^β

$$f^\beta \cdot C^{tc}(t_m) - \overline{C^{ss}}(d^\beta) = 0 \quad (3)$$

723 The scaling factor for the time course experiment
724 follows as

$$f^\beta = \frac{\overline{C^{ss}}(d^\beta)}{C^{tc}(t_m)} \quad (4)$$

725 4.9 Model inputs

726 The SBML model was generated by specifying
727 initial concentrations, rate expressions, parameter
728 values, and compartmental volumes as the model
729 inputs, see Fig. 2I.

730 *Volume.* The physical volume of the cytoplasmic
731 compartment and the β -cell volume were obtained
732 from the values reported in a morphometric study
733 of β -cells (Dean, 1973).

734 *Initial concentrations.* The initial concentrations
735 of glycolytic intermediates were obtained from
736 the mean curve $\overline{C^{ss}}$ (Sec. 2.1) at a basal glucose
737 concentration of 3 mM. The initial value of glucose
738 in the external/blood compartment is 3 mM.

The initial concentrations of cofactors were
739 expressed as polynomial functions passing through
740 the data points of the mean curve, which is computed
741 as the weighted average of data normalized
742 experimental curves (Sec. 2.1). In the SBML model,
743 the polynomial expressions were defined using
744 assignment rules. 745

Kinetic constants. The median values of the
746 half-saturation or Michaelis-Menten constants K_m
747 (Sec. 4.5), were assigned to the model parameters. 748

Equilibrium constants. The values of the
749 equilibrium constants K_{eq} were collected
750 from NIST (Goldberg and Tewari, 2003) and
751 EQUILIBRATOR (Noor et al., 2013). 752

Model equations. For all the glycolytic reactions,
753 the biochemical interactions were expressed using
754 modular rate laws (Liebermeister et al., 2010) of the
755 form Eq. 5. 756

$$v = \frac{V_{max} \prod_i a_i (1 - \frac{\Gamma}{K_{eq}})}{\prod_i (1 + a_i) + \prod_j (1 + b_j) - 1} \quad (5)$$

Here, a_i is S_i/Km_s , b_i is P_i/Km_p , S refers to
757 the substrate and P refers to the product. K_{eq} is
758 the equilibrium constant and Γ is the mass-action
759 ratio (Liebermeister et al., 2010). 760

The use of detailed mechanistic rate laws was
761 avoided due to the challenges associated with
762 finding a large number of parameter values. 763

Insulin secretion was modeled via a
764 phenomenological equation depending on
765 ATP/ADP ratio. The insulin release flux given
766 by Eq. 6, is characterized by three parameters,
767 the maximal rate of insulin release V_{max} , the Hill
768 coefficient n , and K_m the ratio of ATP/ADP that
769 results in half-maximal insulin release. 770

$$v^{IRS} = V_{max}^{IRS} \frac{\left(\frac{ATP}{ADP}\right)^n}{\left(K_m\right)^n + \left(\frac{ATP}{ADP}\right)^n} \quad (6)$$

Boundary metabolites and reactions. Species in the external and mitochondrial compartments were assumed to be boundary species with constant concentrations, i.e. glucose and lactate in the external compartment and pyruvate in the mitochondrial compartment were held constant. Some boundary reactions were modeled as irreversible reactions, i.e. the export of lactate and the transport of pyruvate in the mitochondrion.

Metabolites determined by rate rules. To account for glucose-dependent changes in the concentrations of phosphate, NAD, and NADH, polynomial functions were used to express the concentrations as rate rules. This approach ensured that the concentration of fixed metabolites in the system increased as a function of glucose dose.

Changes in total adenine nucleotides. The sum of adenine nucleotides ($ATP + ADP = ATP_{tot}$) changes with glucose. To account for these changes, a reaction ΔATP was added that changes the total ATP according to the observed steady-state data for a given glucose value (Eq. 7).

$$\Delta ATP = f(ATP_{tot}(glc) - (ATP + ADP)) \quad (7)$$

The $ATP_{tot}(glc)$ values are determined by the interpolating polynomial of the mean steady-state glucose dose response of the ATP+ADP data.

4.10 Model calibration

The normalized time-course and steady-state data was used for model calibration and parameter estimation (Fig. 2J). An overview of the subset of data used for model calibration is shown in Fig. 1. The following data were not used: NADH and NAD were fixed metabolites in the model, with NAD/NADH and NADH+NAD calculated from the metabolites. Total ATP was calculated by summing ATP and ADP, and ATP ratio was calculated by finding the ratio. The insulin secretion rate (IRS) was used to derive the parameters of the IRS function.

A subset of the V_{max} parameters was optimized to minimize the error between model predictions and

experimental observations. The cost function is given by the sum of squares of residuals

$$F(\mathbf{P}) = \sum_{\alpha,s} (\mathbf{c}_s^\alpha - \mathbf{c}_s^M(\mathbf{P}))^2 \quad (8)$$

In Eq. 8, \mathbf{c}_s^α is the concentration of the metabolite s in the experiment α and \mathbf{c}_s^M is the concentration of the metabolite s predicted by the model M . \mathbf{P} is the set of 16 parameters of maximum reaction rates V_{max} . The experimental data of all transient metabolites in the model were stored in spreadsheets. The parameter estimation simulation experiments were set up using basiCO (Bergmann, 2023), the Python interface of COPASI (Hoops et al., 2006). The incubation glucose concentration and incubation time were mapped to the independent variable (glc_{ext} , glucose in the external compartment) and model time, respectively. The transient metabolites were assigned to the model elements as dependent variables. The mean values of V_{max} calculated from the curated values of the enzyme activities were assigned as initial values. The lower and upper bounds specified for the reaction rates V_{max} were set to 0 and 10000, respectively. The calculations were performed using Cloud-COPASI, the front-end to a computer cluster at the Centre for Cell Analysis and Modelling. Cloud-COPASI is an extension of Condor-COPASI (Kent et al., 2012). 400 iterations of parameter estimation were performed on Cloud-COPASI using the SRES algorithm, a global optimization method. The optimal values of the parameter set were obtained from the iteration that yielded the minimum objective value and updated in the model.

4.11 Kinetic model and model predictions

All information was written into the model, validation was performed using sbmlutils, and model simulations were performed, see Fig. 2K, L.

Finally, we performed model predictions of glycolytic intermediates and insulin response as a function of varying glucose concentrations. The set of differential equations was numerically integrated using basiCO (Bergmann, 2023) based on COPASI (Hoops et al., 2006) and sbmlsim (König, 2021) based on libroadrunner (Welsh et al., 2023; Somogyi et al.,

850 2015). For the glucose dose-response, glucose was
851 varied as `linspace(0.01, 35, num=11)` and
852 the model was simulated to steady-state. For the time
853 course simulations, glucose was varied identically and
854 simulations were run for 60 min. Simulations were
855 performed either with COPASI or independently using
856 libroadrunner to ensure reproducibility of key model
857 results.

858 The model is available in SBML ([Hucka et al., 2019](#); [Keating et al., 2020](#)) under a CC-BY 4.0 license
859 from <https://github.com/matthiaskoenig/pancreas-model>. In this study, version 0.9.5 of the model is
860 presented ([Deepa Maheshvare and König, 2023](#)).

CONFLICT OF INTEREST STATEMENT

863 The authors declare no competing interests.

AUTHOR CONTRIBUTIONS

864 DM, SR, MK, and DP conceived and designed the
865 study. DM and MK developed and implemented the
866 computational model and data normalization workflow,
867 and performed the analysis. DM curated the experimental
868 data, performed parameter estimation, and drafted
869 the initial version of the manuscript. All authors
870 read, discussed the results, revised, and approved the
871 manuscript.

FUNDING

872 Research of DM was supported by the Senior Research
873 Fellowship from the Ministry of Human Resource
874 Development (MHRD), Government of India. MK
875 was supported by the Federal Ministry of Education
876 and Research (BMBF, Germany) within the research
877 network Systems Medicine of the Liver (LiSyM,
878 grant number 031L0054) and ATLAS (grant number
879 031L0304B) and by the German Research Foundation
880 (DFG) within the Research Unit Program FOR 5151
881 "QuaLiPerF (Quantifying Liver Perfusion-Function
882 Relationship in Complex Resection - A Systems
883 Medicine Approach)" by grant number 436883643 and
884 grant number 465194077 (Priority Programme SPP
885 2311, Subproject SimLivA). This work was supported
886 by the BMBF-funded de.NBI Cloud within the German

Network for Bioinformatics Infrastructure (de.NBI) 887
(031A537B, 031A533A, 031A538A, 031A533B, 888
031A535A, 031A537C, 031A534A, 031A532B). 889

ACKNOWLEDGMENTS

DM thanks Dr. Murthy Madiraju S.R., Montreal Diabetes 890
Research Center, CRCHUM, Montréal, Canada, Dr. 891
Pedro Mendes, University of Connecticut, and Dr. Frank 892
Bergmann, University of Heidelberg for the invaluable 893
discussions. Access to Cloud-COPASI is supported by 894
NIH Grant R24 GM137787 from the National Institute 895
for General Medical Sciences. 896

REFERENCES

- Akhtar, M. S., Verspohl, E., Hegner, D., and 897
Ammon, H. P. (1977). 6-Phosphogluconate/glucose- 898
6-phosphate ratio in rat pancreatic islets during 899
inhibition of insulin release by exogenous insulin. 900
Diabetes 26, 857–863. doi:10.2337/diab.26.9.857 901
- Alcazar, O. and Buchwald, P. (2019). Concentration- 902
Dependency and Time Profile of Insulin Secretion: 903
Dynamic Perifusion Studies With Human and Murine 904
Islets. *Frontiers in Endocrinology* 10, 680. doi:10.905
3389/fendo.2019.00680 906
- Ammon, H. P., Bacher, M., Brändle, W. F., Waheed, A., 907
Roenfeldt, M., el-Sayed, M. E., et al. (1998). Effect of 908
forty-eight-hour glucose infusion into rats on islet ion 909
fluxes, ATP/ADP ratio and redox ratios of pyridine 910
nucleotides. *The Journal of Endocrinology* 156, 583– 911
590. doi:10.1677/joe.0.1560583 912
- Ammon, H. P., Hoppe, E., Akhtar, M. S., and 913
Niklas, H. (1979). Effect of leucine on the 914
pyridine nucleotide contents of islets and on the 915
insulin released–interactions in vitro with methylene 916
blue, thiol oxidants, and p-chloromercuribenzoate. 917
Diabetes 28, 593–599. doi:10.2337/diab.28.6.593 918
- Ashcroft, F. M. (2006). K(ATP) channels and 919
insulin secretion: A key role in health and disease. 920
Biochemical Society Transactions 34, 243–246. doi: 921
10.1042/BST20060243 922
- Ashcroft, S. J., Capito, K., and Hedeskov, C. J. 923
(1973a). Time course studies of glucose-induced 924

- 925 changes in glucose-6-phosphate and fructose-1,6-
926 diphosphate content of mouse and rat pancreatic islets.
927 *Diabetologia* 9, 299–302. doi:10.1007/BF01221858
928
- 928 Ashcroft, S. J. and Christie, M. R. (1979). Effects of
929 glucose on the cytosolic ration of reduced/oxidized
930 nicotinamide-adenine dinucleotide phosphate in rat
931 islets of Langerhans. *The Biochemical Journal* 184,
932 697–700. doi:10.1042/bj1840697
- 933 Ashcroft, S. J., Hedeskov, C. J., and Randle, P. J. (1970).
934 Glucose metabolism in mouse pancreatic islets. *The
935 Biochemical Journal* 118, 143–154. doi:10.1042/
936 bj1180143
- 937 Ashcroft, S. J., Weerasinghe, L. C., and Randle,
938 P. J. (1973b). Interrelationship of islet metabolism,
939 adenosine triphosphate content and insulin release.
940 *The Biochemical Journal* 132, 223–231. doi:10.1042/
941 bj1320223
- 942 Bergmann, F. T. (2023). basico: a simplified python
943 interface to COPASI doi:10.5281/zenodo.7541481
- 944 Bertram, R., Pedersen, M. G., Luciani, D. S., and
945 Sherman, A. (2006). A simplified model for
946 mitochondrial ATP production. *Journal of theoretical
947 biology* 243, 575–586
- 948 Bertram, R., Sherman, A., and Satin, L. S.
949 (2007). Metabolic and electrical oscillations:
950 partners in controlling pulsatile insulin secretion.
951 *American Journal of Physiology-Endocrinology And
952 Metabolism* 293, E890–E900
- 953 Brun, T., Roche, E., Assimacopoulos-Jeannet, F.,
954 Corkey, B. E., Kim, K. H., and Prentki, M. (1996).
955 Evidence for an anaplerotic/malonyl-CoA pathway in
956 pancreatic beta-cell nutrient signaling. *Diabetes* 45,
957 190–198. doi:10.2337/diab.45.2.190
- 958 Corkey, B. E., Glennon, M. C., Chen, K. S., Deeney, J. T.,
959 Matschinsky, F. M., and Prentki, M. (1989). A role for
960 malonyl-CoA in glucose-stimulated insulin secretion
961 from clonal pancreatic beta-cells. *The Journal of
962 Biological Chemistry* 264, 21608–21612
- 963 Cote, R., Reisinger, F., Martens, L., Barsnes, H.,
964 Vizcaino, J. A., and Hermjakob, H. (2010). The
965 Ontology Lookup Service: Bigger and better. *Nucleic
966 Acids Research* 38, W155–W160. doi:10.1093/nar/
967 gkq331
- 968 Courtot, M., Juty, N., Knüpfer, C., Waltemath, D.,
969 Zhukova, A., Dräger, A., et al. (2011). Controlled
vocabularies and semantics in systems biology. *Molecular Systems Biology* 7, 543. doi:10.1038/msb.2011.77
- 970 Dean, P. M. (1973). Ultrastructural morphometry of the
971 pancreatic β -cell. *Diabetologia* 9, 115–119. doi:10.1007/BF01230690
- 972 Deepa Maheshvare, M. and König, M. (2023). Model of
973 glucose-stimulated insulin secretion in the pancreatic
974 β -Cell doi:10.5281/zenodo.7711084
- 975 Detimary, P., Dejonghe, S., Ling, Z., Pipeleers, D.,
976 Schuit, F., and Henquin, J. C. (1998). The changes in
977 adenine nucleotides measured in glucose-stimulated
978 rodent islets occur in beta cells but not in alpha
979 cells and are also observed in human islets. *The
980 Journal of Biological Chemistry* 273, 33905–33908.
981 doi:10.1074/jbc.273.51.33905
- 982 Detimary, P., Van den Berghe, G., and Henquin, J. C.
983 (1996). Concentration dependence and time course
984 of the effects of glucose on adenine and guanine
985 nucleotides in mouse pancreatic islets. *The Journal
986 of Biological Chemistry* 271, 20559–20565. doi:10.
987 1074/jbc.271.34.20559
- 988 Di Camillo, B., Eduati, F., Nair, S. K., Avogaro, A., and
989 Toffolo, G. M. (2014). Leucine modulates dynamic
990 phosphorylation events in insulin signaling pathway
991 and enhances insulin-dependent glycogen synthesis
992 in human skeletal muscle cells. *BMC cell biology* 15,
993 9. doi:10.1186/1471-2121-15-9
- 994 Ebrahim, A., Beber, M. E., Mandal, S., König, M.,
995 Redestig, H., Diener, C., et al. (2023). opencobra/cobrapy: 0.26.2
996 doi:10.5281/zenodo.7502407
- 997 Ewart, R. B., Yousufzai, S. Y., Bradford, M. W., and
998 Shrago, E. (1983). Rat islet mitochondrial adenine
999 nucleotide translocase and the regulation of insulin
1000 secretion. *Diabetes* 32, 793–797. doi:10.2337/diab.
1001 32.9.793
- 1002 Fridlyand, L. E. and Philipson, L. H. (2010). Glucose
1003 sensing in the pancreatic beta cell: A computational
1004 systems analysis. *Theoretical Biology and Medical
1005 Modelling* 7, 15. doi:10.1186/1742-4682-7-15
- 1006 Fritzsche, L., Weigert, C., Häring, H.-U., and Lehmann,
1007 R. (2008). How insulin receptor substrate
1008 proteins regulate the metabolic capacity of the
1009 liver—implications for health and disease. *Current
1010 Medicine* 10, 1014–1022. doi:10.1007/s11671-008-9370-2

- 1015 Medicinal Chemistry 15, 1316–1329. doi:10.2174/
1016 092986708784534956
- 1017 Gelbach, P. E., Zheng, D., Fraser, S. E., White, K. L.,
1018 Graham, N. A., and Finley, S. D. (2022). Kinetic
1019 and data-driven modeling of pancreatic β -cell central
1020 carbon metabolism and insulin secretion. *PLoS
1021 computational biology* 18, e1010555
- 1022 Giroix, M. H., Sener, A., Pipeleers, D. G., and Malaisse,
1023 W. J. (1984). Hexose metabolism in pancreatic islets.
1024 Inhibition of hexokinase. *The Biochemical Journal*
1025 223, 447–453. doi:10.1042/bj2230447
- 1026 Goldberg, R. and Tewari, Y. (2003). *Thermodynamics
1027 of Enzyme-Catalyzed Reactions* (McGraw Hill, New
1028 York, NY)
- 1029 Grzegorzewski, J., Bartsch, F., Köller, A., and König,
1030 M. (2021a). Pharmacokinetics of Caffeine: A
1031 Systematic Analysis of Reported Data for Application
1032 in Metabolic Phenotyping and Liver Function Testing.
1033 *Frontiers in Pharmacology* 12, 752826. doi:10.3389/
1034 fphar.2021.752826
- 1035 Grzegorzewski, J., Brandhorst, J., Green, K.,
1036 Eleftheriadou, D., Duport, Y., Barthorscht, F., et al.
1037 (2021b). PK-DB: Pharmacokinetics database for
1038 individualized and stratified computational modeling.
1039 *Nucleic Acids Research* 49, D1358–D1364. doi:10.
1040 1093/nar/gkaa990
- 1041 Guay, C., Joly, E., Pepin, E., Barbeau, A., Hentsch,
1042 L., Pineda, M., et al. (2013). A role for cytosolic
1043 isocitrate dehydrogenase as a negative regulator of
1044 glucose signaling for insulin secretion in pancreatic
1045 ss-cell. *PloS One* 8, e77097. doi:10.1371/journal.
1046 pone.0077097
- 1047 Guerrero-Hernandez, A. and Verkhratsky, A. (2014).
1048 Calcium signalling in diabetes. *Cell Calcium* 56, 297–
1049 301. doi:10.1016/j.ceca.2014.08.009
- 1050 Hari, A. and Lobo, D. (2022). mergem: merging
1051 and comparing genome-scale metabolic models using
1052 universal identifiers. *bioRxiv*
- 1053 Hedeskov, C. J., Capito, K., and Thams, P. (1987).
1054 Cytosolic ratios of free [NADPH]/[NADP+] and
1055 [NADH]/[NAD+] in mouse pancreatic islets, and
1056 nutrient-induced insulin secretion. *The Biochemical
1057 Journal* 241, 161–167. doi:10.1042/bj2410161
- Hoops, S., Sahle, S., Gauges, R., Lee, C., Pahle, J.,
1058 Simus, N., et al. (2006). COPASI—a complex
1059 pathway simulator. *Bioinformatics* 22, 3067–3074
- Huang, M. and Joseph, J. W. (2014). Assessment
1061 of the metabolic pathways associated with glucose-
1062 stimulated biphasic insulin secretion. *Endocrinology*
1063 155, 1653–1666. doi:10.1210/en.2013-1805
- Hucka, M., Bergmann, F. T., Chaouiya, C., Dräger,
1065 A., Hoops, S., Keating, S. M., et al. (2019).
1066 The Systems Biology Markup Language (SBML):
1067 Language Specification for Level 3 Version 2 Core
1068 Release 2. *Journal of Integrative Bioinformatics* 16,
1069 20190021. doi:10.1515/jib-2019-0021
- Hucka, M., Nickerson, D. P., Bader, G. D., Bergmann,
1071 F. T., Cooper, J., Demir, E., et al. (2015). Promoting
1072 Coordinated Development of Community-Based
1073 Information Standards for Modeling in Biology: The
1074 COMBINE Initiative. *Frontiers in Bioengineering
1075 and Biotechnology* 3, 19. doi:10.3389/fbioe.2015.1076
00019
- Jiang, N., Cox, R. D., and Hancock, J. M. (2007).
1077 A kinetic core model of the glucose-stimulated
1079 insulin secretion network of pancreatic β cells.
1080 *Mammalian Genome* 18, 508–520. doi:10.1007/
1081 s00335-007-9011-y
- Johnson, D., Shepherd, R. M., Gill, D., Gorman, T.,
1083 Smith, D. M., and Dunne, M. J. (2007). Glucose-
1084 dependent modulation of insulin secretion and
1085 intracellular calcium ions by GKA50, a glucokinase
1086 activator. *Diabetes* 56, 1694–1702. doi:10.2337/
1087 db07-0026
- Keating, S. M., Waltemath, D., König, M., Zhang, F.,
1089 Dräger, A., Chaouiya, C., et al. (2020). SBML Level
1090 3: An extensible format for the exchange and reuse
1091 of biological models. *Molecular Systems Biology* 16,
1092 e9110. doi:10.15252/msb.20199110
- Kent, E., Hoops, S., and Mendes, P. (2012).
1094 Condor-COPASI: High-throughput computing for
1095 biochemical networks. *BMC systems biology* 6, 91.
1096 doi:10.1186/1752-0509-6-91
- King, Z. A., Lu, J., Dräger, A., Miller, P., Federowicz,
1098 S., Lerman, J. A., et al. (2016). BiGG Models: A
1099 platform for integrating, standardizing and sharing
1100 genome-scale models. *Nucleic Acids Research* 44,
1101 D515–522. doi:10.1093/nar/gkv1049

- 1103 König, M., Bulik, S., and Holzhütter, H.-G. (2012a).
 1104 Quantifying the contribution of the liver to glucose
 1105 homeostasis: A detailed kinetic model of human
 1106 hepatic glucose metabolism. *PLoS computational*
 1107 *biology* 8, e1002577. doi:10.1371/journal.pcbi.
 1108 1002577
- 1109 König, M., Dräger, A., and Holzhütter, H.-G.
 1110 (2012b). Cysbml: a cytoscape plugin for SBML.
 1111 *Bioinformatics* 28, 2402–2403
- 1112 König, M. (2021). sbmlsim: SBML simulation made
 1113 easy doi:10.5281/zenodo.5531088
- 1114 König, M. (2022a). brendapy: BRENDA parser in
 1115 python doi:10.5281/zenodo.6555202
- 1116 König, M. (2022b). pymetadata: Python utilities for
 1117 SBML doi:10.5281/zenodo.7432576
- 1118 König, M. (2022c). sbmlutils: Python utilities for SBML
 1119 doi:10.5281/zenodo.7462781
- 1120 Lamontagne, J., Pepin, E., Peyot, M.-L., Joly, E.,
 1121 Ruderman, N. B., Poitout, V., et al. (2009).
 1122 Pioglitazone acutely reduces insulin secretion and
 1123 causes metabolic deceleration of the pancreatic
 1124 beta-cell at submaximal glucose concentrations.
 1125 *Endocrinology* 150, 3465–3474. doi:10.1210/en.
 1126 2008-1557
- 1127 Liebermeister, W., Uhlendorf, J., and Klipp, E.
 1128 (2010). Modular rate laws for enzymatic reactions:
 1129 Thermodynamics, elasticities and implementation.
 1130 *Bioinformatics (Oxford, England)* 26, 1528–1534.
 1131 doi:10.1093/bioinformatics/btq141
- 1132 Liu, Y. Q., Moibi, J. A., and Leahy, J. L. (2004). Chronic
 1133 high glucose lowers pyruvate dehydrogenase activity
 1134 in islets through enhanced production of long chain
 1135 acyl-CoA: Prevention of impaired glucose oxidation
 1136 by enhanced pyruvate recycling through the malate-
 1137 pyruvate shuttle. *The Journal of Biological Chemistry*
 1138 279, 7470–7475. doi:10.1074/jbc.M307921200
- 1139 Liu, Y. Q., Tornheim, K., and Leahy, J. L. (1998). Fatty
 1140 acid-induced beta cell hypersensitivity to glucose.
 1141 Increased phosphofructokinase activity and lowered
 1142 glucose-6-phosphate content. *Journal of Clinical*
 1143 *Investigation* 101, 1870–1875. doi:10.1172/JCI1211
- 1144 MacDonald, P. E., Joseph, J. W., and Rorsman, P.
 1145 (2005). Glucose-sensing mechanisms in pancreatic
 1146 beta-cells. *Philosophical Transactions of the Royal*
Society of London. Series B, Biological Sciences 360, 2211–2225. doi:10.1098/rstb.2005.1762
- 1147 Malaisse, W. J., Hutton, J. C., Kawazu, S., and Sener,
 1148 A. (1978). The stimulus-secretion coupling of
 1149 glucose-induced insulin release. Metabolic effects of
 1150 menadione in isolated islets. *European Journal of*
Biochemistry 87, 121–130. doi:10.1111/j.1432-1033.1978.tb12357.x
- 1151 Malaisse, W. J. and Sener, A. (1987). Glucose-induced
 1152 changes in cytosolic ATP content in pancreatic islets.
Biochimica Et Biophysica Acta 927, 190–195. doi:10.1016/0167-4889(87)90134-0
- 1153 Malinowski, R. M., Ghiasi, S. M., Mandrup-Poulsen,
 1154 T., Meier, S., Lerche, M. H., Ardenkjær-Larsen,
 1155 J. H., et al. (2020). Pancreatic β -cells respond
 1156 to fuel pressure with an early metabolic switch.
Scientific Reports 10, 15413. doi:10.1038/s41598-020-72348-1
- 1157 Malmgren, S., Spégel, P., Danielsson, A. P. H., Nagorny,
 1158 C. L., Andersson, L. E., Nitert, M. D., et al.
 1159 (2013). Coordinate changes in histone modifications,
 1160 mRNA levels, and metabolite profiles in clonal INS-
 1161 832/13 β -cells accompany functional adaptations to
 1162 lipotoxicity. *The Journal of Biological Chemistry* 288,
 1163 11973–11987. doi:10.1074/jbc.M112.422527
- 1164 Matschinsky, F. M. and Ellerman, J. E. (1968).
 1165 Metabolism of glucose in the islets of Langerhans.
The Journal of Biological Chemistry 243, 2730–2736
- 1166 Matschinsky, F. M., Pagliara, A. S., Stillings, S. N.,
 1167 and Hover, B. A. (1976). Glucose and ATP levels
 1168 in pancreatic islet tissue of normal and diabetic rats.
The Journal of Clinical Investigation 58, 1193–1200.
 1169 doi:10.1172/JCI108572
- 1170 McKenna, J. P., Dhumpa, R., Mukhitov, N., Roper,
 1171 M. G., and Bertram, R. (2016). Glucose Oscillations
 1172 Can Activate an Endogenous Oscillator in Pancreatic
 1173 Islets. *PLOS Computational Biology* 12, e1005143.
 1174 doi:10.1371/journal.pcbi.1005143
- 1175 Meglasson, M. D. and Matschinsky, F. M. (1986).
 1176 Pancreatic islet glucose metabolism and regulation
 1177 of insulin secretion. *Diabetes/Metabolism Reviews* 2,
 1178 163–214. doi:10.1002/dmr.5610020301
- 1179 Meglasson, M. D., Nelson, J., Nelson, D., and Erecinska,
 1180 M. (1989). Bioenergetic response of pancreatic
 1181 islets to stimulation by fuel molecules. *Metabolism*:
 1182

- 1192 Clinical and Experimental 38, 1188–1195. doi:10.1193/0026-0495(89)90158-3
- 1193 Merrins, M. J., Bertram, R., Sherman, A., and Satin, L. S. (2012). Phosphofructo-2-kinase/Fructose-2,6-bisphosphatase Modulates Oscillations of Pancreatic Islet Metabolism. *PLoS ONE* 7, e34036. doi:10.1371/journal.pone.0034036
- 1194 Miwa, I., Ichimura, N., Sugiura, M., Hamada, Y., and Taniguchi, S. (2000). Inhibition of glucose-induced insulin secretion by 4-hydroxy-2-nonenal and other lipid peroxidation products. *Endocrinology* 141, 2767–2772. doi:10.1210/endo.141.8.7614
- 1195 Neal, M. L., Gennari, J. H., Waltemath, D., Nickerson, D. P., and König, M. (2020). Open modeling and exchange (OMEX) metadata specification version 1.0. *Journal of Integrative Bioinformatics* 17, 20200020. doi:10.1515/jib-2020-0020
- 1196 Neal, M. L., König, M., Nickerson, D., Misirli, G., Kalbasi, R., Dräger, A., et al. (2019). Harmonizing semantic annotations for computational models in biology. *Briefings in Bioinformatics* 20, 540–550. doi:10.1093/bib/bby087
- 1197 Newsholme, P., Cruzat, V., Arfuso, F., and Keane, K. (2014). Nutrient regulation of insulin secretion and action. *Journal of Endocrinology* 221, R105–R120. doi:10.1530/JOE-13-0616
- 1198 Noor, E., Haraldsdóttir, H. S., Milo, R., and Fleming, R. M. T. (2013). Consistent Estimation of Gibbs Energy Using Component Contributions. *PLoS Computational Biology* 9, e1003098. doi:10.1371/journal.pcbi.1003098
- 1199 Noronha, A., Modamio, J., Jarosz, Y., Guerard, E., Sompairac, N., Preciat, G., et al. (2019). The Virtual Metabolic Human database: Integrating human and gut microbiome metabolism with nutrition and disease. *Nucleic Acids Research* 47, D614–D624. doi:10.1093/nar/gky992
- 1200 Pedersen, M. G., Corradin, A., Toffolo, G. M., and Cobelli, C. (2008). A subcellular model of glucose-stimulated pancreatic insulin secretion. *Philosophical Transactions. Series A, Mathematical, Physical, and Engineering Sciences* 366, 3525–3543. doi:10.1098/rsta.2008.0120
- 1201 Placzek, S., Schomburg, I., Chang, A., Jeske, L., Ulbrich, M., Tillack, J., et al. (2017). BRENDA in 2017: New perspectives and new tools in BRENDA. *Nucleic Acids Research* 45, D380–D388. doi:10.1093/nar/gkw952
- 1202 Prentki, M., Matschinsky, F. M., and Madiraju, S. M. (2013). Metabolic Signaling in Fuel-Induced Insulin Secretion. *Cell Metabolism* 18, 162–185. doi:10.1016/j.cmet.2013.05.018
- 1203 Rohatgi, A. (2021). Webplotdigitizer: Version 4.5
- 1204 Rorsman, P. and Braun, M. (2013). Regulation of insulin secretion in human pancreatic islets. *Annual Review of Physiology* 75, 155–179. doi:10.1146/annurev-physiol-030212-183754
- 1205 Salvucci, M., Neufeld, Z., and Newsholme, P. (2013). Mathematical Model of Metabolism and Electrophysiology of Amino Acid and Glucose Stimulated Insulin Secretion: In Vitro Validation Using a β -Cell Line. *PLoS ONE* 8, e52611. doi:10.1371/journal.pone.0052611
- 1206 Sauro, H. M. (2020). *Systems Biology: Introduction to Pathway Modeling* (Ambrosius Publishing)
- 1207 Sener, A., Hutton, J. C., Kawazu, S., Boschero, A. C., Somers, G., Devis, G., et al. (1978). The stimulus-secretion coupling of glucose-induced insulin release. Metabolic and functional effects of NH₄⁺ in rat islets. *The Journal of Clinical Investigation* 62, 868–878. doi:10.1172/JCI109199
- 1208 Sener, A., Van Schaftingen, E., Van de Winkel, M., Pipeleers, D. G., Malaisse-Lagae, F., Malaisse, W. J., et al. (1984). Effects of glucose and glucagon on the fructose 2,6-bisphosphate content of pancreatic islets and purified pancreatic B-cells. A comparison with isolated hepatocytes. *The Biochemical Journal* 221, 759–764. doi:10.1042/bj2210759
- 1209 Smolen, P. (1995). A model for glycolytic oscillations based on skeletal muscle phosphofructokinase kinetics. *Journal of Theoretical Biology* 174, 137–148. doi:10.1006/jtbi.1995.0087
- 1210 Sener, A., Bouteiller, J.-M., Glazier, J. A., König, M., Medley, J. K., Swat, M. H., et al. (2015). libRoadRunner: A high performance SBML simulation and analysis library. *Bioinformatics (Oxford, England)* 31, 3315–3321. doi:10.1093/bioinformatics/btv363
- 1211 Spégel, P., Andersson, L. E., Storm, P., Sharoyko, V., Göhring, I., Rosengren, A. H., et al. (2015). Unique

- 1282 and Shared Metabolic Regulation in Clonal β -Cells
1283 and Primary Islets Derived From Rat Revealed by
1284 Metabolomics Analysis. *Endocrinology* 156, 1995–
1285 2005. doi:10.1210/en.2014-1391
- 1286 Spégl, P., Sharoyko, V. V., Goehring, I., Danielsson,
1287 A. P. H., Malmgren, S., Nagorny, C. L. F., et al.
1288 (2013). Time-resolved metabolomics analysis of β -
1289 cells implicates the pentose phosphate pathway in the
1290 control of insulin release. *The Biochemical Journal*
1291 450, 595–605. doi:10.1042/BJ20121349
- 1292 Sugden, M. C. and Ashcroft, S. J. (1977).
1293 Phosphoenolpyruvate in rat pancreatic islets:
1294 A possible intracellular trigger of insulin release?
1295 *Diabetologia* 13, 481–486. doi:10.1007/BF01234500
- 1296 Taniguchi, S., Okinaka, M., Tanigawa, K., and
1297 Miwa, I. (2000). Difference in mechanism
1298 between glyceraldehyde- and glucose-induced insulin
1299 secretion from isolated rat pancreatic islets. *Journal
1300 of Biochemistry* 127, 289–295. doi:10.1093/
1301 oxfordjournals.jbchem.a022606
- 1302 The UniProt Consortium (2017). UniProt: The universal
1303 protein knowledgebase. *Nucleic Acids Research* 45,
1304 D158–D169. doi:10.1093/nar/gkw1099
- 1305 Tornheim, K. (1997). Are metabolic oscillations
1306 responsible for normal oscillatory insulin secretion?
1307 *Diabetes* 46, 1375–1380
- 1308 Trus, M., Warner, H., and Matschinsky, F. (1980).
1309 Effects of glucose on insulin release and on
1310 intermediary metabolism of isolated perfused
1311 pancreatic islets from fed and fasted rats. *Diabetes* 29,
1312 1–14. doi:10.2337/diab.29.1.1
- 1313 Trus, M. D., Hintz, C. S., Weinstein, J. B., Williams,
1314 A. D., Pagliara, A. S., and Matschinsky, F. M.
1315 (1979). A comparison of the effects of glucose
1316 and acetylcholine on insulin release and intermediary
1317 metabolism in rat pancreatic islets. *The Journal of
1318 Biological Chemistry* 254, 3921–3929
- 1319 Welsh, C., Xu, J., Smith, L., König, M., Choi, K., and
1320 Sauro, H. M. (2023). libRoadRunner 2.0: A high
1321 performance SBML simulation and analysis library.
1322 *Bioinformatics (Oxford, England)* 39, btac770. doi:10.
1323 1093/bioinformatics/btac770
- 1324 Westermark, P. O., Kotaleski, J. H., Björklund, A.,
1325 Grill, V., and Lansner, A. (2007). A mathematical
1326 model of the mitochondrial NADH shuttles and
anaplerosis in the pancreatic beta-cell. *American
1327 journal of physiology. Endocrinology and metabolism* 1328
292, E373–93. doi:10.1152/ajpendo.00589.2005
- 1329 Wittig, U., Rey, M., Weidemann, A., Kania, R., and
1330 Müller, W. (2018). SABIO-RK: An updated resource
1331 for manually curated biochemical reaction kinetics.
1332 *Nucleic Acids Research* 46, D656–D660. doi:10.1093/
1333 nar/gkx1065
- 1334 Woods, S. C., Lutz, T. A., Geary, N., and Langhans,
1335 W. (2006). Pancreatic signals controlling food
1336 intake; insulin, glucagon and amylin. *Philosophical
1337 Transactions of the Royal Society of London. Series
1338 B, Biological Sciences* 361, 1219–1235. doi:10.1098/
1339 rstb.2006.1858
- 1340 Xu, J., Han, J., Long, Y. S., Epstein, P. N., and Liu,
1341 Y. Q. (2008a). The role of pyruvate carboxylase in
1342 insulin secretion and proliferation in rat pancreatic
1343 beta cells. *Diabetologia* 51, 2022–2030. doi:10.1007/
1344 s00125-008-1130-9
- 1345 Xu, J., Han, J., Long, Y. S., Lock, J., Weir, G. C., Epstein,
1346 P. N., et al. (2008b). Malic enzyme is present in mouse
1347 islets and modulates insulin secretion. *Diabetologia*
1348 51, 2281–2289. doi:10.1007/s00125-008-1155-0

Table 1. Overview of studies reporting concentrations of metabolites used for model calibration.

Study	PMID	Metabolites	Species	Measurement	Steady-state	Time course	Citation
Akhtar1977	19330	G6P	Wistar rats	Absolute	✓		Akhtar et al. (1977)
Alcazar2019	31632354	IRS	Human, C57BL6/J mice	Absolute	✓	✓	Alcazar and Buchwald (2019)
Ammon1979	36318	NAD, NADH/NAD, NADH+NAD, NADH	Wistar rats	Absolute	✓	✓	Ammon et al. (1979)
Ammon1998	9582515	NAD, ATP/ADP, NADH, NADH+NAD, IRS, NADH/NAD	Wistar rats	Absolute	✓		Ammon et al. (1998)
Ashcroft1970	4919469	G6P	Albino mice	Absolute	✓		Ashcroft et al. (1970)
Ashcroft1973	4148924	ATP, IRS	White mice	Absolute	✓	✓	Ashcroft et al. (1973a)
Ashcroft1973b	4199014	G6P	Theillers original strain mice, Wistar rats	Absolute	✓	✓	Ashcroft et al. (1973b)
Ashcroft1979	44196	PYR	Wistar rats	Absolute	✓		Ashcroft and Christie (1979)
Brun1996	8549864	IRS	HIT-T15 β -cell line	Absolute	✓	✓	Brun et al. (1996)
Corkey1989	2689441	IRS	HIT β -cell line	Absolute	✓		Corkey et al. (1989)
Detimary1996	8702800	ATP, ADP, ATP+ADP, ATP/ADP, IRS	NMRI mice	Absolute	✓	✓	Detimary et al. (1996)
Detimary1998	9852040	ATP, ADP, ATP+ADP, ATP/ADP	Wistar rats	Absolute	✓		Detimary et al. (1998)
Ewart1983	6313455	PEP, IRS	Sprague-Dawley rats	Absolute	✓		Ewart et al. (1983)
Giroix1984	6388570	PEP, IRS	Albino rats	Absolute	✓		Giroix et al. (1984)
Guay2013	24130841	DHAP, ATP, PYR, LAC, NADH/NAD, IRS	INS 832/13 β -cell line	Relative	✓		Guay et al. (2013)
Hedeskov1987	3551925	PYR, LAC, NADH/NAD, IRS,	Theillers original strain mice	Absolute	✓		Hedeskov et al. (1987)
Huang2014	24564396	G6P, DHAP, PG3, PYR, LAC	INS 832/13 β -cell line	Absolute	✓	✓	Huang and Joseph (2014)
Johnson2007	17360975	IRS	Human, Sprague-Dawley rats, C57BL6 mice, MIN6 β -cell line	Absolute	✓		Johnson et al. (2007)
Lamontagne2009	19406947	APT, IRS	INS 832/13 β -cell line	Relative	✓		Lamontagne et al. (2009)
Liu1998	9576750	G6P, IRS	Sprague-Dawley rats	Absolute	✓		Liu et al. (1998)
Liu2004	14660628	G6P, PYR, IRS	Sprague-Dawley rats	Absolute	✓		Liu et al. (2004)
Malaisse1977	27353	ATP, ADP, ATP+ADP, ATP/ADP, NAD, NADH, NADH+NAD, NADH/NAD	Albino rats	Absolute	✓		Malaisse et al. (1978)
Malaisse1987	2434137	ATP, ADP, ATP+ADP, ATP/ADP	Albino rats	Absolute	✓		Malaisse and Sener (1987)
Malinowski2020	32963286	PYR, LAC	INS-1 β -cell line	Relative	✓		Malinowski et al. (2020)
Malmgren2013	23476019	GLC, G6P, DHAP, PG3, PYR, LAC	INS-1 832/13 β -cell line	Relative	✓		Malmgren et al. (2013)
Matschinsky1968	4870741	GLC, G6P, FBP, ATP	Mice	Absolute	✓		Matschinsky and Ellerman (1968)
Matschinsky1976	136453	GLC, ATP	Sprague-Dawley rats	Absolute	✓		Matschinsky et al. (1976)
Meglasson1986	2943567	F26P	Rats	Absolute	✓		Meglasson and Matschinsky (1986)
Miwa2000	10919261	G6P, F6P, FBP, GRAP, DHAP	Wistar rats	Absolute	✓		Meglasson et al. (1989)
Sener1978	29912	NAD, NADH, NADH+NAD	Albino rats	Absolute	✓		Sener et al. (1978)
Sener1984	6383351	F26BP	Albino rats	Absolute	✓	✓	Sener et al. (1984)
Spégel2013	23282133	PG2, PG3, PEP, PYR, LAC	INS-1 832/13 β -cell line	Relative	✓	✓	Spégel et al. (2013)
Spégel2015	25774549	G6P, ATP, PG2, PG3, PEP, PYR, LAC, IRS	INS-1 832/13 β -cell line	Relative	✓	✓	Spégel et al. (2015)
Sugden1977	332570	PEP	Albino Wistar rats	Absolute	✓		Sugden and Ashcroft (1977)
Taniguchi2000	10731696	G6P, F6P, FBP, GRAP, DHAP, ATP	Wistar rats	Absolute	✓	✓	Taniguchi et al. (2000)
Trus1979	220227	G6P, NADH, PHOS, IRS	Rats	Absolute	✓	✓	Trus et al. (1979)
Trus1980	6991311	G6P, ATP, ADP, ATP+ADP, NADH, PHOS, IRS	Holtzman rats	Absolute	✓	✓	Trus et al. (1980)
Xu2008a	18769905	IRS	Sprague-Dawley rats	Absolute	✓		Xu et al. (2008a)
Xu2008b	18802677	IRS	C57BL/6 mice, Sprague-Dawley rats, MIN-6 β -cell line	Absolute	✓		Xu et al. (2008b)

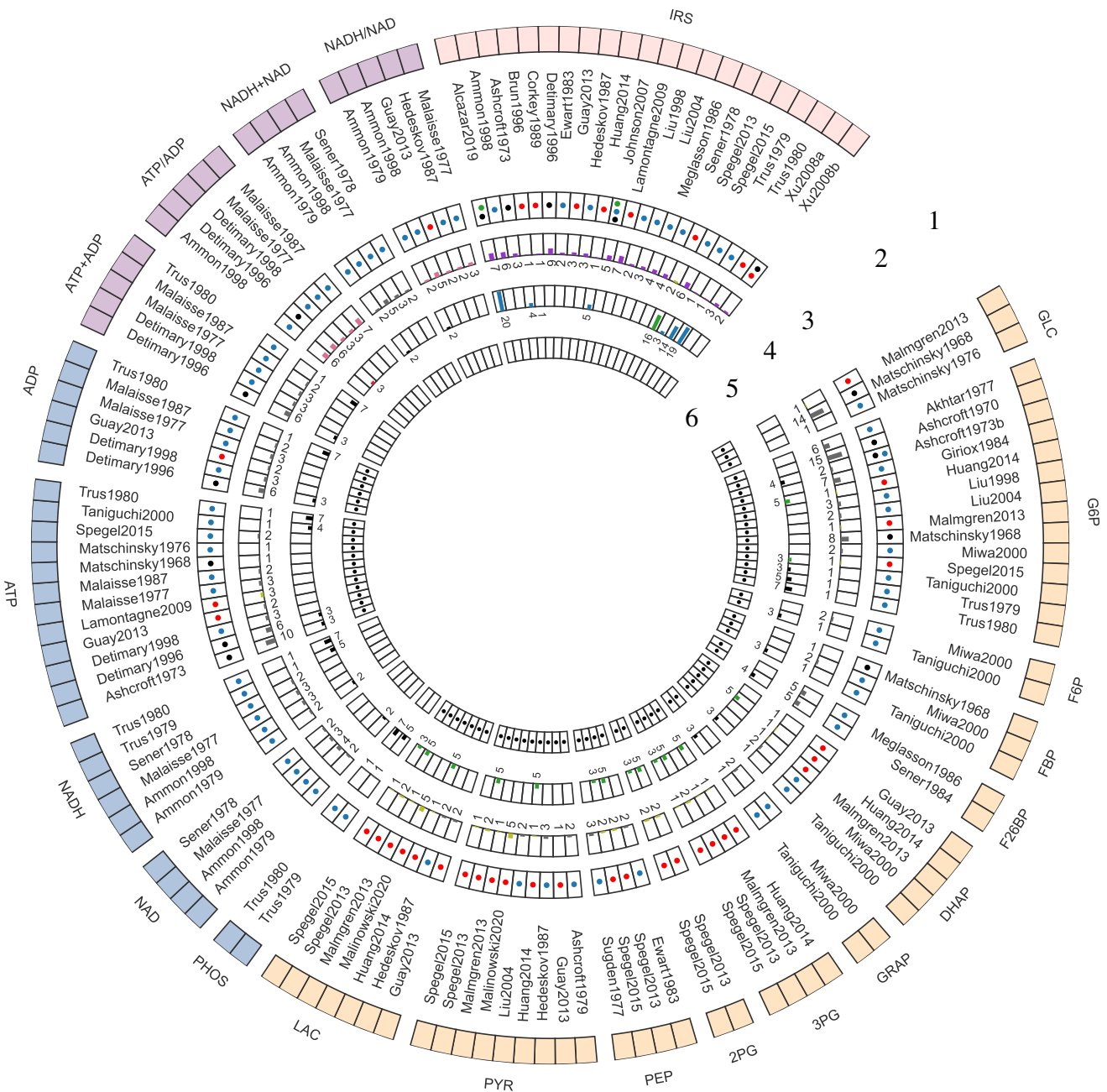


Figure 1. Curated data for model development and evaluation. The data description is detailed from the periphery to the center of the Circos plot. **1. Model elements:** The outermost layer provides an overview of the metabolites included in the data set. GLC: glucose, G6P: glucose 6-phosphate, F6P: fructose 6-phosphate, FBP: fructose 1,6-bisphosphate, F26BP: fructose 2,6-bisphosphate, DHAP: dihydroxyacetone phosphate, GRAP: glyceraldehyde 3-phosphate, BPG: 1,3-biphosphoglycerate, 3PG: 3-phosphoglycerate, 2PG: 2-phosphoglycerate, PEP: phosphoenolpyruvate, PYR: pyruvate, LAC: lactate, PHOS: phosphate, NAD: nicotinamide adenine dinucleotide, NADH: reduced nicotinamide adenine dinucleotide, NADH total: NADH + NAD; NADH ratio: NADH/NAD; ATP: adenosine triphosphate, ADP: adenosine diphosphate, ATP total: ATP + ADP, ATP ratio: ATP/ADP, IRS: insulin secretion rate. The metabolites were grouped in the following categories: Color code: • glycolytic intermediates, • cofactors, • cofactor ratio or sum, • insulin secretion rate (IRS); **2. Studies:** The second layer depicts the islet-cell specific metabolite profiling studies curated from the literature; **3. Animal species:** The third layer indicates the animal species or cell line from which the data was curated. Color code: • Rat, • Human, • Mouse, and • Cell line data; **4. time course data:** The fourth layer shows a bar graph illustrating the number of data points collected from studies reporting time course data of metabolites. Color code: • relative (or fold), • concentration, • ratio, • rate measurements; **5. Steady-state data:** The fifth layer indicates the number of data points collected from studies reporting steady-state/ dose-response data of metabolites. Color code: • relative (or fold), • concentration, • ratio, • rate measurements; **6. Data used for parameter estimation:** The innermost layer indicates the subset of data used for parameter fitting.

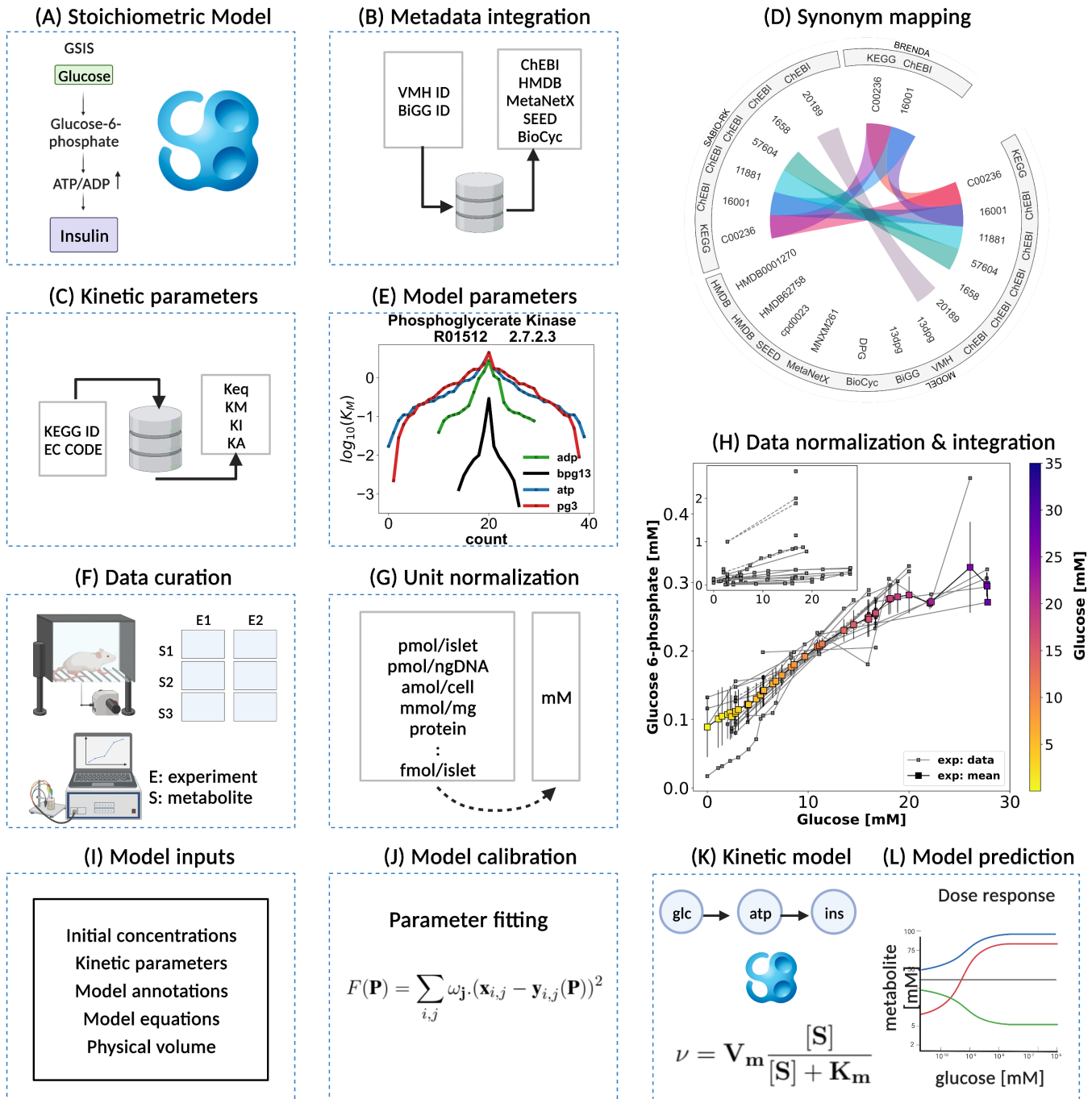


Figure 2. Kinetic model development workflow. (A) Initial stoichiometric model in SBML. Glycolytic reactions were collected from VMH database and existing models of glycolysis. (B) Metadata integration. VMH and BiGG database field identifiers were used to retrieve additional metadata such as HMDB, BioCyc, MetaNetX, ChEBI, and SEED database field identifiers. (C) Synonym mapping. The synonyms associated with each metabolite were queried using compound identifier mapping services. (D) Kinetic parameters. EC number and KEGG reaction identifiers were used to query half-saturation/Michaelis-Menten K_M , inhibition K_I , activation K_A , and equilibrium K_{eq} constants (synonym mapping was applied for all compounds). (E) Model parameters. The parameter values retrieved from different databases were merged and median values were assigned to the model parameters; (F) Data curation. A systematic literature search was performed and metabolite concentrations from islet cell studies were curated. (G) Unit normalization. Absolute and relative quantification of metabolite concentrations reported in heterogeneous units were converted to mM. (H) Data normalization. Systematic bias observed in the unit-normalized data was removed by performing least-squares minimization to minimize the distance between the mean curve of the unit-normalized data curves and the experimental curves of the unit-normalized data. (I) Model inputs. Values of kinetic parameters, initial concentrations, volumes, equations, and annotations have been assigned to the model entities. (J) Model calibration. Time course and steady-state data were used for parameter estimation. (K) Kinetic SBML model. The final kinetic SBML model was generated. (L) Model prediction. Glycolytic intermediates and insulin response were predicted as a function of varying glucose concentrations. Created with BioRender.com.

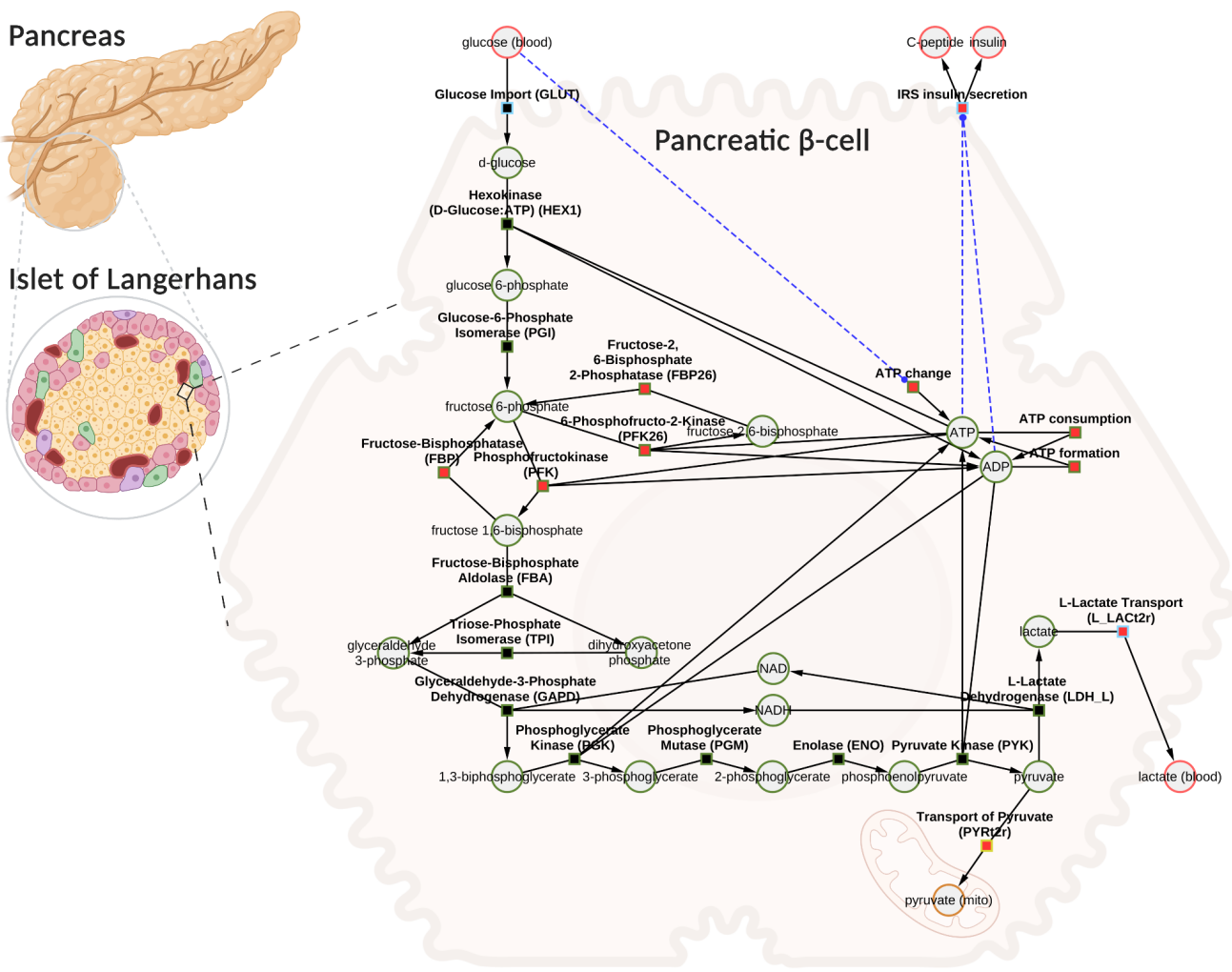


Figure 3. Computational model of glucose-stimulated insulin secretion (GSIS) in the pancreatic β-cell. The model consists of glycolysis and insulin secretion coupled to the energy state (ATP/ADP ratio). The GLUT transporter facilitates the uptake of glucose from the plasma into the cell. Glucose undergoes phosphorylation and the subsequent reactions lead to the production of pyruvate. Pyruvate can either be converted to lactate and exported into blood or transported to the mitochondria where it serves as a fuel source for the production of tricarboxylic acid cycle (TCA) intermediates (the TCA cycle has not been modeled). Depending on the external glucose concentrations, glycolysis intermediates and energy metabolites such as ATP, ADP, NAD, and NADH change. An increase in the ATP/ADP ratio as a result of changes in glucose triggers the cascade of signaling mechanisms that promote insulin secretion by the pancreatic β-cell. Phosphate, water, and hydrogen ions have been omitted from the diagram for clarity (but are included in the model for mass and charge balance). The network diagram was created using CySBML (König et al., 2012b). Created with BioRender.com.

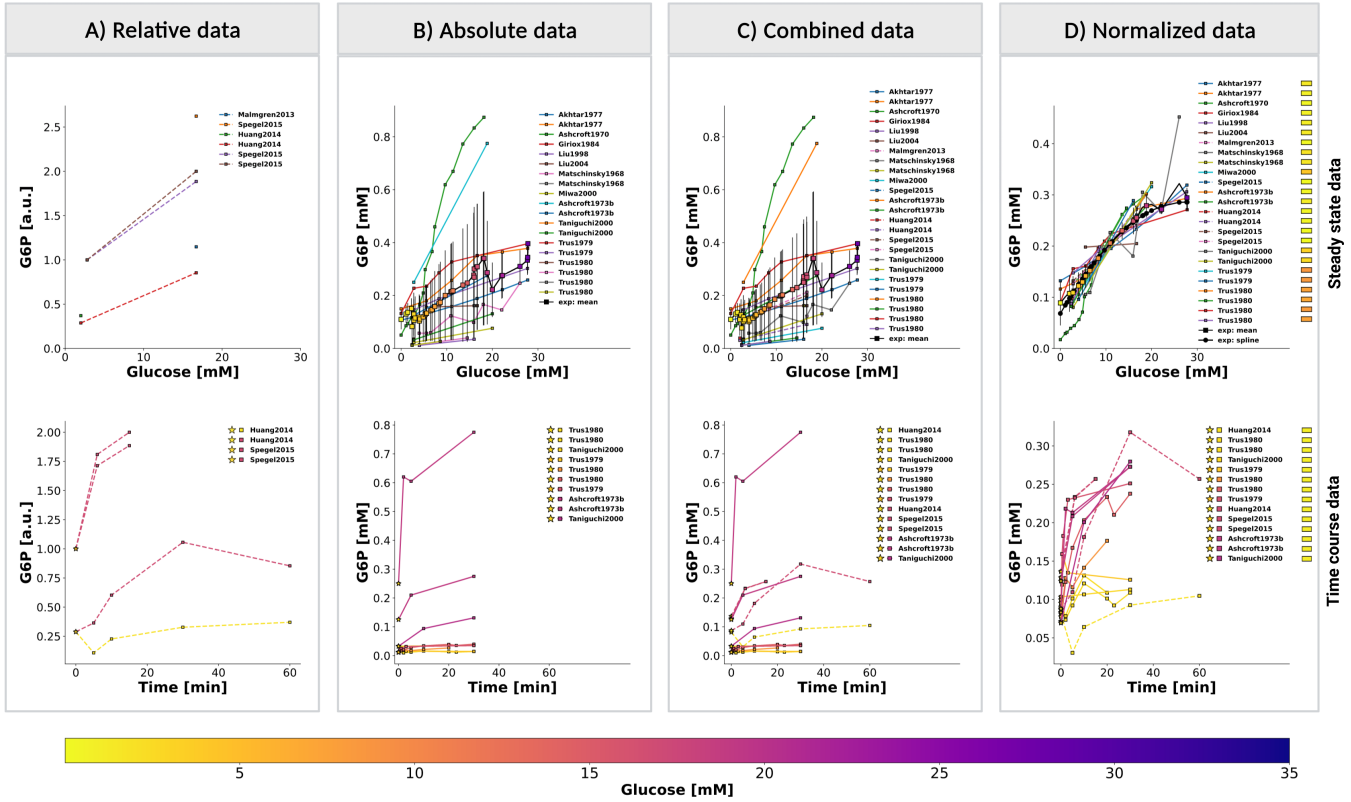


Figure 4. Normalization of steady-state and time course data for glucose 6-phosphate (G6P). (A) Relative data. Experimental curves from β -cell studies reporting relative levels of G6P, expressed as fold to baseline value; **(B) Absolute data.** Experimental curves from β -cell studies reporting absolute concentrations of G6P, the plot displays the unit-normalized absolute data. **(C) Combined data.** The relative (fold) measurements were converted to absolute units and combined with the unit-normalized absolute data. **(D) Normalized data.** Systematic biases between different studies of the combined data were removed by data normalization. Data normalization was performed by minimizing the offset (sum of squared residuals) between the mean curve and the experimental curves. The *mean curve* was computed as the weighted average of the experimental curves and *spline curve* is the piecewise-polynomial interpolation of the data points in the mean curve. For steady-state data, the legend indicates studies associated with the experimental curves. For time course data, the legend indicates the pre-incubation glucose dose (\star), incubation glucose dose (\square), experimental study, and the value of scale transformation parameter f^α (\square) of experiment α . *(top panel)* and *(bottom panel)* show the data of dose-response and time course experiments, respectively. Data from (Akhtar et al., 1977; Ashcroft et al., 1970, 1973b; Giroix et al., 1984; Huang and Joseph, 2014; Liu et al., 1998, 2004; Malmgren et al., 2013; Matschinsky and Ellerman, 1968; Miwa et al., 2000; Spégel et al., 2015; Taniguchi et al., 2000; Trus et al., 1979, 1980). For more details, please refer to Sec. 2.1.

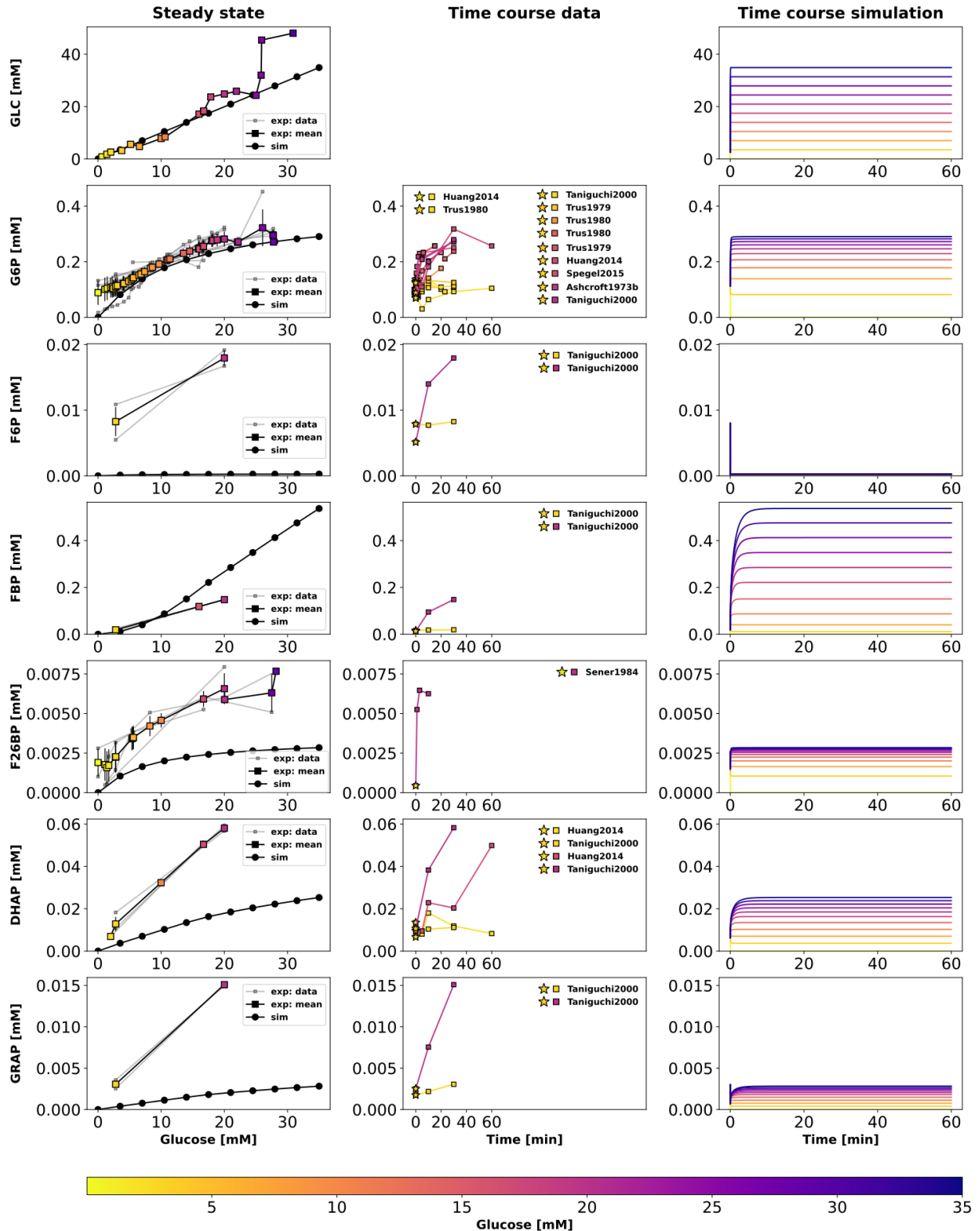


Figure 5. Effect of variations in blood glucose on glycolytic intermediates. (left column) Dose-response simulations. Glucose scan was performed for the calculation of steady-state concentration of metabolites in the model. The steady-state concentrations predicted by the model at various glucose doses were compared with the normalized values of experimental measurements; (middle column) Time course experimental data. Time course values of glycolytic intermediates and cofactors from multiple experimental studies carried out at different incubation doses of glucose; (\star) in the legend indicates the pre-incubation glucose dose. (right column) Time course simulations. The effect of variation in blood glucose dose on the transient concentration of metabolites. GLC: glucose, G6P: glucose 6-phosphate, F6P: fructose 6-phosphate, FBP: fructose 1,6-bisphosphate, F26BP: fructose 2,6-bisphosphate, DHAP: dihydroxyacetone phosphate, GRAP: glyceraldehyde 3-phosphate. Data from (Akhtar et al., 1977; Ashcroft et al., 1970, 1973b; Giroix et al., 1984; Huang and Joseph, 2014; Liu et al., 1998, 2004; Malmgren et al., 2013; Matschinsky and Ellerman, 1968; Miwa et al., 2000; Spégl et al., 2015; Sener et al., 1984; Taniguchi et al., 2000; Trus et al., 1979, 1980).

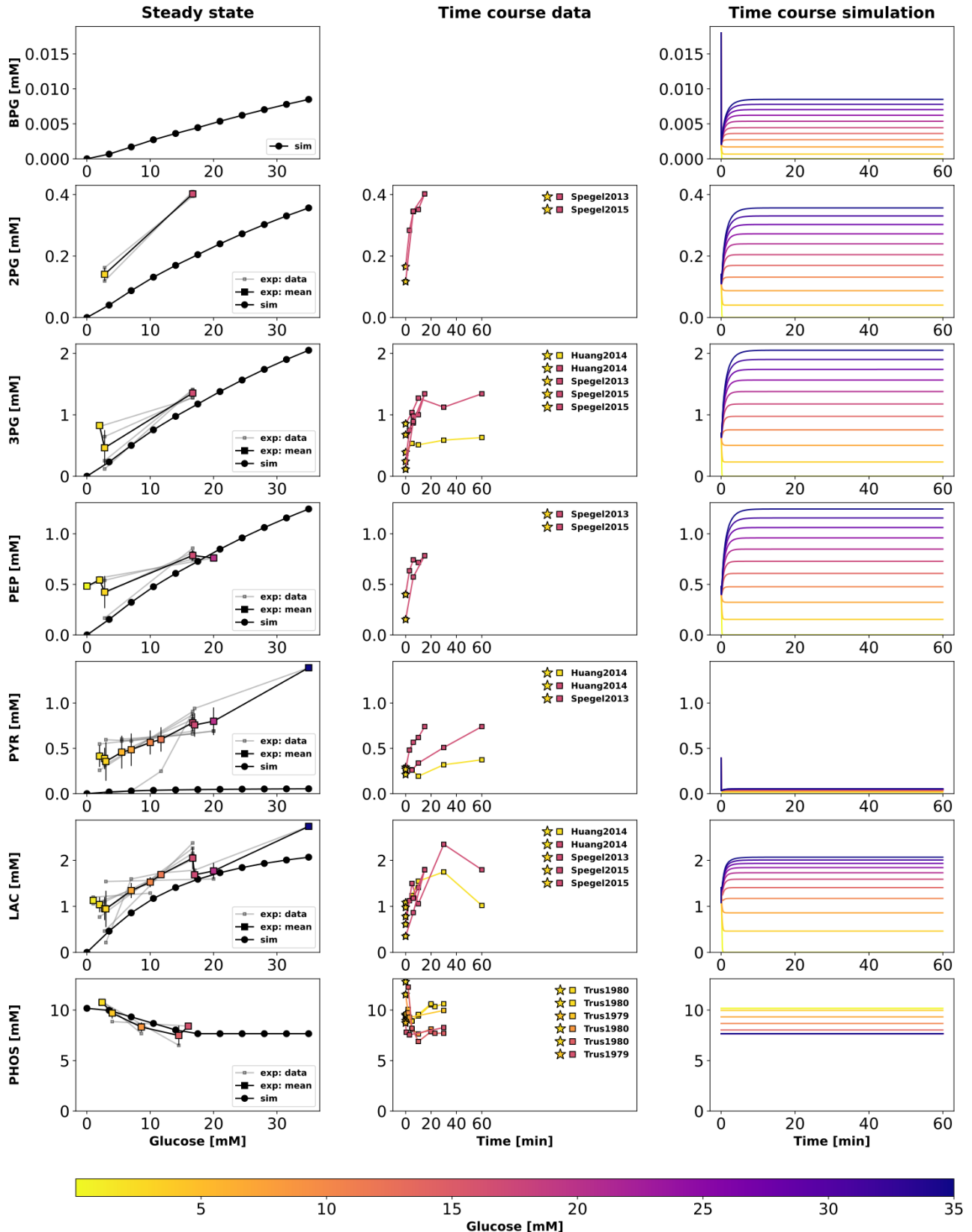


Figure 6. Effect of variations in blood glucose on glycolytic intermediates. The plot is analogous to Fig. 5. BPG: 1,3-biphosphoglycerate, 2PG: 2-phosphoglycerate, 3PG: 3-phosphoglycerate, PEP: phosphoenolpyruvate, PYR: pyruvate, LAC: lactate, PHOS: phosphate. Data from (Ashcroft and Christie, 1979; Ewart et al., 1983; Guay et al., 2013; Hedeskov et al., 1987; Huang and Joseph, 2014; Malinowski et al., 2020; Malmgren et al., 2013; Spégel et al., 2013, 2015; Sugden and Ashcroft, 1977; Trus et al., 1979, 1980).

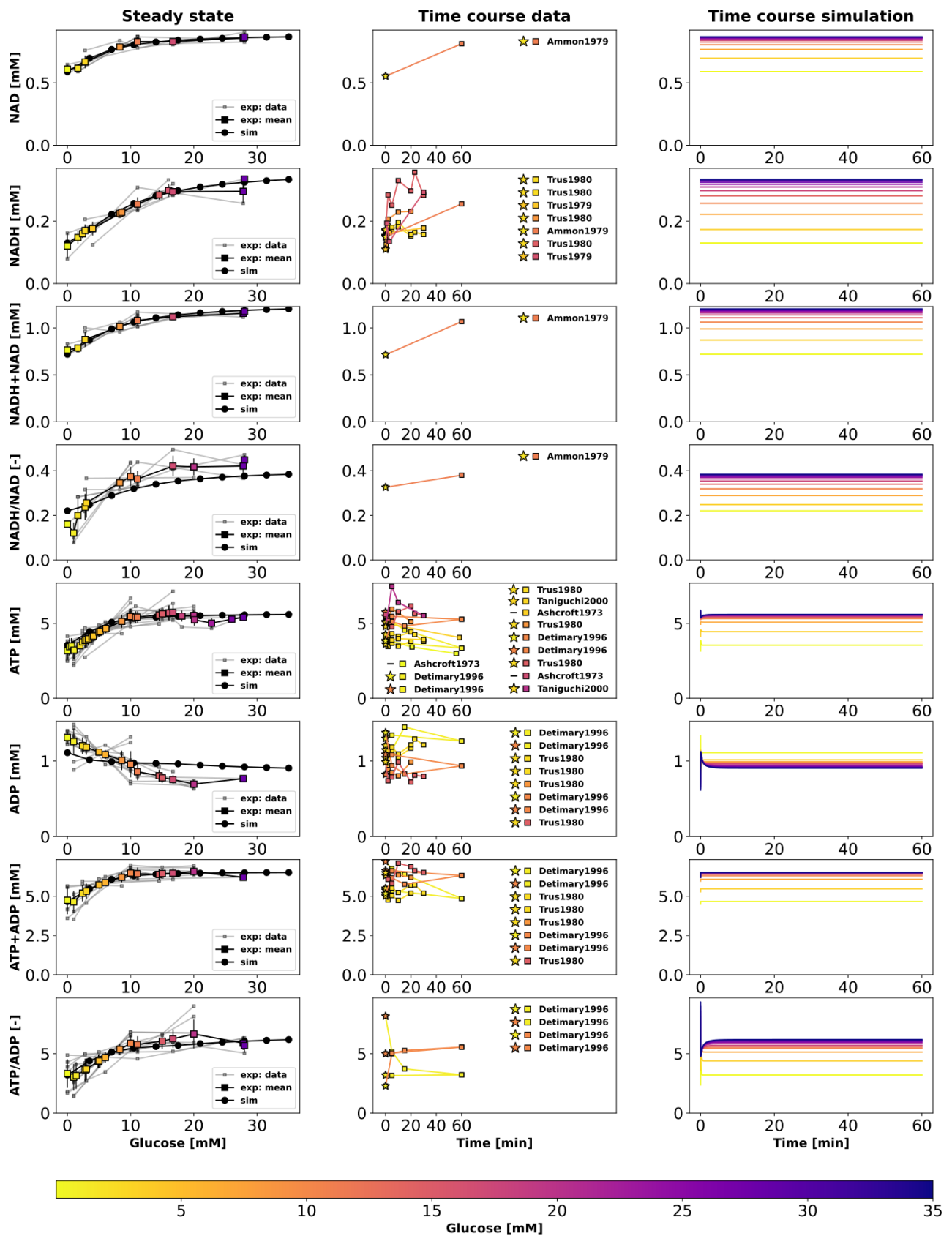


Figure 7. Effect of variations in blood glucose on glycolytic cofactors. The plot is analogous to Fig. 5. NAD: nicotinamide adenine dinucleotide, NADH: nicotinamide adenine dinucleotide reduced. ATP: adenosine triphosphate, ADP: adenosine diphosphate Data from (Ammon et al., 1979, 1998; Ashcroft et al., 1970; Detimary et al., 1996, 1998; Guay et al., 2013; Hedeskov et al., 1987; Lamontagne et al., 2009; Malaisse et al., 1978; Malaisse and Sener, 1987; Matschinsky and Ellerman, 1968; Matschinsky et al., 1976; Sener et al., 1978; Spégel et al., 2015; Taniguchi et al., 2000; Trus et al., 1979, 1980).

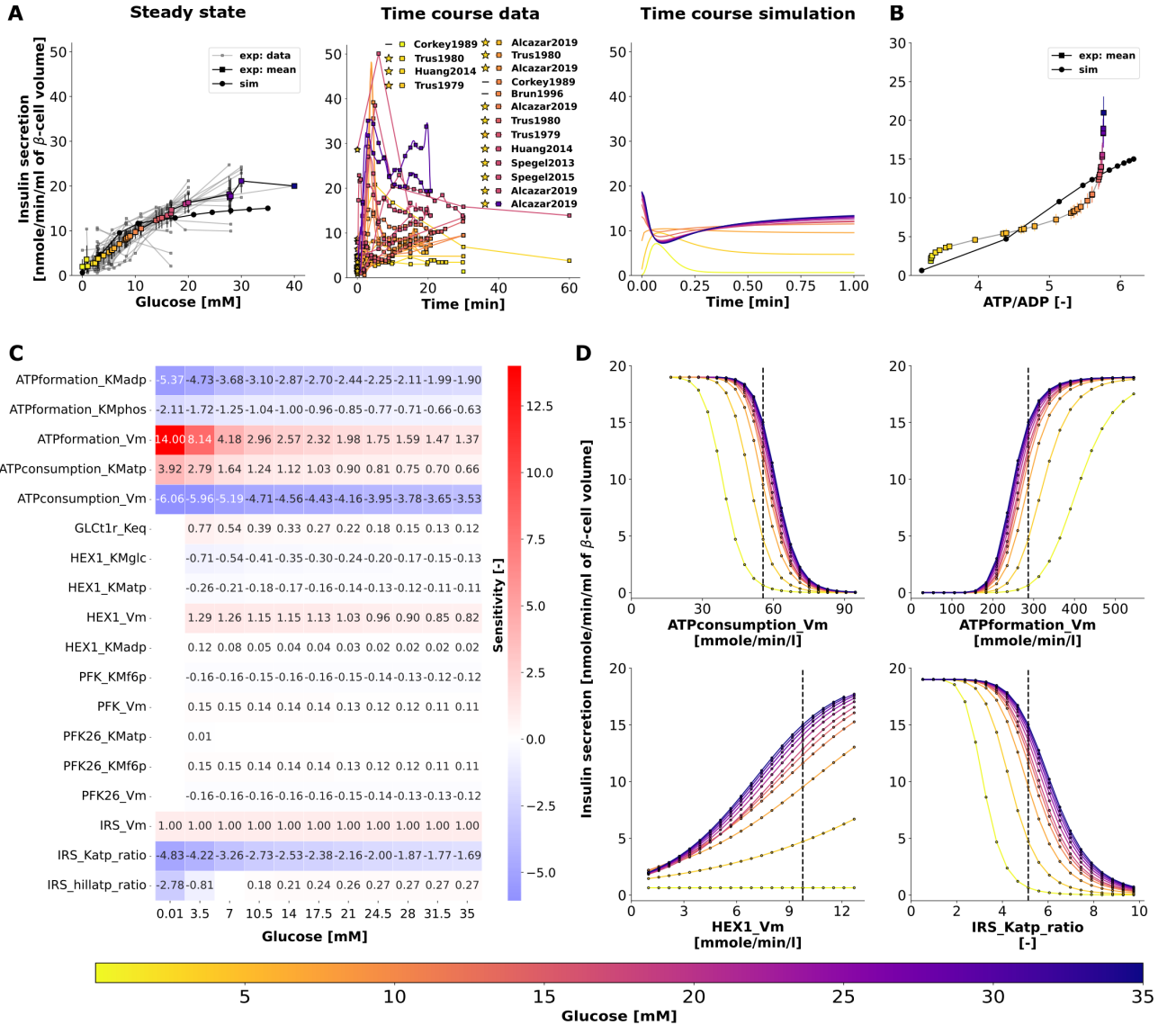


Figure 8. (A) Effect of variations in blood glucose on insulin secretion. The plot is analogous to Fig. 5. Data from (Alcazar and Buchwald, 2019; Ammon et al., 1998; Ashcroft et al., 1973a; Brun et al., 1996; Corkey et al., 1989; Detimary et al., 1996, 1998; Ewart et al., 1983; Guay et al., 2013; Hedeskov et al., 1987; Huang and Joseph, 2014; Johnson et al., 2007; Lamontagne et al., 2009; Liu et al., 1998, 2004; Meglasson and Matschinsky, 1986; Sener et al., 1978; Spégel et al., 2013, 2015; Trus et al., 1979, 1980; Xu et al., 2008a,b). (B) Effect of change in energy state (ATP/ADP ratio) of the β -cell on insulin secretion. The rate of insulin release in response to changes in ATP/ADP ratio is shown. (C) Sensitivity analysis indicating the effect of perturbation in model parameters on insulin secretion. Heatmap illustrating the values of scaled local sensitivities illustrating the effect of parameter perturbations on the amount of insulin secretion at varying glucose doses. Highly sensitive values are colored in red and blue. The parameters which cause less than 1% change in insulin response for 10% perturbation were not displayed for clarity. For more details, please refer to Sec. 2.6. (D) Effect of change in model parameters on insulin secretion as a function of glucose dose. The rate of insulin secretion in response to perturbation in the values of ATPconsumption_Vm, HEX1_Vm, IRS_Katp_ratio, IRS_hillKatp_ratio. The vertical line indicates the model value.